Food & Function

ROYAL SOCIETY OF CHEMISTRY

PAPER

Published on 06 August 2026

Cite this: *Food Funct.*, 2026, **17**, 7748

Blue turmeric (*Curcuma caesia* Roxb.): phenolic profile, bioaccessibility after *in vitro* gastrointestinal digestion, and chondroprotective effects in IL-1β-stimulated human chondrocytes.

Michela Battistelli, †[a] Giovanni Caprioli, †[b] Elena Barbieri,†[a] Agnese Santanatoglia,[b] Federico Gianfanti, *[a] Michele Mari, [a] Michele Retini, [a] Maria Assunta Meli,[a] Carla Roselli,[a] Fabio Ferrini,[a] Riham Osman,[a] Sabrina Burattini,[a] Francesco Onesimo[a] and Matteo Micucci *[a]

Received 15th May 2026,
Accepted 31st July 2026

DOI: 10.1039/d6fo02399a

rsc.li/food-function

Osteoarthritis (OA) is a chronic degenerative joint disease characterized by progressive cartilage breakdown driven by inflammatory and oxidative stress mechanisms. Blue turmeric (*Curcuma caesia* Roxb.), a rare and understudied spice, represents a source of bioactive compounds with anti-inflammatory properties. This study aimed to characterize the phenolic profile of a blue turmeric rhizome extract (BTE) and its bioaccessible fraction obtained after *in vitro* gastrointestinal digestion, and to assess their biological effects on human chondrocytes (C-28/I2) exposed to interleukin-1 β (IL-1β). HPLC-MS/MS analyses revealed a phytochemical profile rich in phenolic acids and flavan-3-ols, with partial stability maintained after *in vitro* digestion. Pre-treatment with both native BTE and digested BTE (dBTE) protected chondrocytes against IL-1β-induced cytotoxicity, mitochondrial dysfunction, and nuclear factor erythroid 2-related factor 2 (Nrf2) inactivation. Furthermore, BTE pre-treatment significantly reduced tumour necrosis factor-α (TNF-α) release and preserved cellular morphology. These findings demonstrate that BTE phenolic compounds are partially bioaccessible and exert chondroprotective effects, supporting further preclinical investigation of BTE as a potential functional ingredient for joint health maintenance and OA prevention strategies.

1. Introduction

Osteoarthritis (OA) is a multifactorial degenerative joint disease characterized by progressive cartilage degradation, synovial inflammation, and altered joint homeostasis. At the cellular level, pro-inflammatory cytokines such as IL-1β and TNF-α promote catabolic signalling in chondrocytes, contributing to extracellular matrix degradation, oxidative stress and mitochondrial dysfunction.[1–9] The OA progression is driven by a complex interplay of *in situ* joint inflammation and systemic metabolic imbalances, underlying its systemic rather than solely localized implications.[10] Current therapeutic strategies primarily focus on symptom management and are effective in reducing pain and inflammation; however, preventive strategies for these conditions remain limited. Several dietary factors, including deficiencies in vitamins D, C, and K, have been associated with an increased risk of OA.[11] In addition, adherence to the Mediterranean diet has been linked to a lower prevalence of OA,[12,13] likely, at least in part, due to the presence of polyphenols.[14] Indeed, these compounds have been shown to modulate inflammation, counteract oxidative damage, and support physiological cartilage turnover.[15] Additionally, polyphenols modulate key molecular pathways that regulate chondrocyte viability, control the expression of pro-inflammatory genes, and contribute to extracellular matrix remodelling.[16–22]

In this context, exploring food substances naturally rich in bioactive compounds, commonly used in several countries, may lead to the identification of functional ingredients with health-promoting effects.[23,24] Previous investigations on polyphenols and food-derived blends have revealed considerable potential for the management of inflammatory conditions;[25–28] however, poor bioaccessibility of these compounds still limits their translational relevance. To address this limitation, several *in vitro* digestion models have been proposed, including the INFOGEST protocol and its modified ver-

[a]*Department of Biomolecular Sciences, University of Urbino Carlo Bo, 61029 Urbino, Italy. E-mail: federico.gianfanti@uniurb.it, matteo.micucci@uniurb.it*
[b]*School of Pharmacy, Chemistry Interdisciplinary Project (ChIP), University of Camerino, Via Madonna delle Carceri 9/B, 62032 Camerino, Italy*
† These authors contributed equally to the work.

sions, the TNO gastrointestinal model, and the DIDGI® system.[29] Previous research from our group has highlighted the biological effects of food-derived blends and isolated compounds on several molecular networks, thereby counteracting the development of maladaptive phenotypes.[30–34] Among polyphenol-rich nutraceuticals, Curcuma represents a valuable source of flavanols and other bioactive constituents with anti-inflammatory and antioxidant properties, making it a promising candidate for the management of inflammatory conditions.[35,36] *Curcuma caesia* Roxb., commonly known as blue turmeric, is a rare species of the *Zingiberaceae* family, native to India, Nepal, and Bangladesh, where it thrives in tropical and subtropical forests. Although less widely used than *Curcuma longa* L., it has been incorporated into traditional culinary practices in specific regions of India. It is typically used as a paste or powder to enhance the colour and aroma of different dishes, particularly in fermented foods and herbal blends. Although it is not currently authorized in Europe, it may be classified as a novel food in the future.[37–39] As previously reported, blue turmeric extracts are characterized by a rich polyphenolic profile, including high levels of epicatechin, ellagic acid, and procyanidins, which have been associated with antioxidant and anti-ageing effects in HaCaT keratinocytes exposed to UVB-induced phototoxicity.[40] Nevertheless, the bioaccessibility of *Curcuma caesia* Roxb. polyphenols has not yet been established, nor has the potential impact of blue turmeric-derived blends on osteoarthritis-related cellular processes. In this context, the present study characterises the bioaccessibility of a polyphenol-rich extract from *Curcuma caesia* Roxb. following *in vitro* simulated gastrointestinal digestion and elucidates its effects on inflammation-related molecular pathways in IL-1β-stimulated human chondrocytes, thereby providing mechanistic insights into its potential as a functional food ingredient for osteoarthritis management.

2. Materials and methods

2.1. Plant material and extraction procedure

The rhizome of *Curcuma caesia* Roxb. was supplied by Bellaria Agricultural Company, Igea Marina (RN, Italy). The material was sliced into thin sections, frozen at −80 °C, and subsequently lyophilized using a LIO5P freeze dryer (Pascale) for 24 h. Subsequently, 2 g of *Curcuma caesia* Roxb. dried powders were extracted with 40 mL of methanol under agitation at 40 °C for 2 h, corresponding to a solid-to-liquid ratio of 1 : 20 (w/v). The liquid fraction was then separated by centrifugation, filtered using Supervelox filter paper, and the solvent was removed with a rotary vacuum evaporator at 40 °C. This extraction process was repeated twice. The obtained extract was freeze-dried and stored at −20 °C in moisture -and light- protected vials until use. The extraction yield of BTE, calculated as the percentage ratio between the dry weight of the freeze-dried extract and the dry weight of the starting dried plant material, was 4.73 ± 0.23%.

2.2. Digestion procedure

In vitro gastrointestinal digestion was employed to evaluate the bioaccessibility of the phytocomplex. The procedure was based on the dynamic model reported by Oomen *et al.*[41] Salivary, gastric, duodenal, and biliary juices were individually prepared to reproduce the complexity of digestive fluids involved in gastrointestinal processing. The exact procedure, including the volumes (mL) and quantities (mg) of the extractants, is fully described by Roselli *et al.*, with slight modifications, and reported in SI Table S4.[29] Briefly, a vial containing 500 mg of the extract was exposed to each digestive fluid under controlled temperature conditions (37 ± 2 °C) and constant agitation (29 rpm), simulating gastrointestinal tract conditions according to the sequence reported in Table 1. The resulting suspension was centrifuged at 4000*g* for 1 h using a VWR MEGA STAR 4.0R centrifuge to separate the digestive juice from the digested sample (pellet). The supernatant was then filtered using a 0.45 μm filter into a clean vial and freeze-dried for 48 h using a LIO 5P freeze dryer. The resulting digested sample was stored at −20 °C until use.

2.3. HPLC-MS/MS determination of BTE and dBTE polyphenolic composition

2.3.1. Reagents and standards. Analytical standards (purity ≥ 95%) of cyanidin-3-glucoside chloride, delphinidin-3,5-diglucoside chloride, delphinidin-3-galactoside chloride, petunidin-3-glucoside chloride, malvidin-3-galactoside chloride, quercetin-3-glucoside and kaempferol-3-glucoside were purchased from PhytoLab (Vestenbergsgreuth, Germany). The remaining 31 analytical standards (purity ≥ 95%) of the 38 phenolic compounds were supplied by Sigma-Aldrich (Milan, Italy). Individual stock solutions of each analyte, at a concentration of 1000 mg L^{-1}, were prepared by dissolving pure standards in HPLC-grade methanol and storing them in glass stoppered bottles at 4 °C, except for anthocyanins, which were stored at −15 °C until analysis. Standard working solutions at various concentrations were prepared daily by appropriate dilution of the stock solutions with HPLC-grade methanol. Formic acid (99%) was obtained from Merck (Darmstadt, Germany). Analytical-grade hydrochloric acid (37%) was obtained from Carlo Erba Reagents (Milan, Italy). HPLC-grade methanol was supplied by Sigma-Aldrich (Milano, Italy). Deionized water (>18 MΩ cm resistivity) was further purified using a Milli-Q SP Reagent Water System (Millipore, Bedford, MA, USA). All

Table 1 Procedure for complete digestion of the BTE extract

Stage	Sample	Extractant	Time (min)
1	BTE extract (500 mg)	0.34 mL salivary solution (pH 6.5 ± 0.2)	5
2	Resulting suspension from stage 1	0.68 mL gastric solution (pH 1.07 ± 0.07)	120
3	Resulting suspension from stage 2	0.68 mL duodenal solution + 0.34 mL biliary solution (pH 8.0 ± 0.2)	120

solvents and solutions were filtered through a 0.2 μm polyamide filter from Sartorius Stedim (Goettingen, Germany). Before HPLC analysis, all samples were filtered with Phenex™ RC 4 mm 0.2 μm syringeless filter, Phenomenex (Castel Maggiore, BO, Italy).

2.3.2. Sample preparation for HPLC-ESI-MS/MS analysis. For the extraction of phenolic compounds, 2 g of the BTE and dBTE were extracted with 10 mL of ethanol: water mixture (70 : 30, v/v) by sonication (FALC ultrasonic bath, Treviglio, Italy) at a frequency of 40 kHz for 60 min. After centrifugation at 5000 rpm for 10 min, the supernatants were filtered through a 0.2 μm syringeless filter before injection into HPLC-MS/MS triple quadrupole. All samples were stored at −15° C until analysis. Each sample was analysed in triplicate.

2.3.3. HPLC-ESI-MS/MS analysis. HPLC-MS/MS studies were performed using an Agilent 1290 Infinity series and a Triple Quadrupole 6420 from Agilent Technology (Santa Clara, CA) equipped with an electrospray ionization (ESI) source operating in negative and positive ionization modes.[42] In fact, the instrument allowed to perform a single run with polarity switching. MS/MS parameters of each analyte were optimized in flow injection analysis (FIA) (1 μL of a 10 mg L^{-1} individual standard solution) by using Optimizer Software (Agilent). The separation of target compounds was achieved on a Synergi Polar-RP C18 analytical column (250 mm × 4.6 mm, 4 μm) from Phenomenex (Chesire, UK). The column was preceded by a Polar RP security guard cartridge (4 mm × 3 mm ID). The mobile phase was a mixture of (A) water and (B) methanol, both with formic acid 0.1%, at a flow rate of 0.8 mL min^{-1} in gradient elution mode. The composition of the mobile phase varied as follows: 0–1 min, isocratic condition, 20% B; 1–25 min, 20–85% B; 25–26 min, isocratic condition, 85% B; 26–32 min, 85–20% B. All solvents and solutions were filtered through a 0.2 μm polyamide filter from Sartorius Stedim (Goettingen, Germany). The injection volume was 2 μL. The temperature of the column was 30 °C, and the temperature of the drying gas in the ionization source was 350 °C. The gas flow was 12 L min^{-1}, the nebulizer pressure was 55 psi, and the capillary voltage was 4.000 V. Detection was performed in the dynamic-multiple reaction monitoring (dynamic-MRM) mode, and the dynamic-MRM peak areas were integrated for quantification. The most abundant product ion was used for quantitation, and the others for qualification. The specific time window for each compound (Δ retention time) was set at 2 min. The selected ion transitions and the mass spectrometer parameters for the analyzed compounds are reported in Table 2. The analytical method was previously validated according to international validation guidelines. Linearity was assessed using eight concentration levels ranging from 0.005 to 10 mg L^{-1}. Limits of detection (LOD) and quantification (LOQ) were determined using signal-to-noise ratios of 3 and 10, respectively. Method precision was evaluated through intra-day and inter-day repeatability tests and expressed as relative standard deviation (RSD%). Recovery experiments were performed through spiking procedures at two concentration levels. Validation parameters for all monitored phenolic compounds are reported in SI Table S3. Quantification was performed by external calibration using authentic analytical standards. No isotope-labelled internal standard was employed.

2.4. Culture of immortalized human chondrocyte cell line

This study evaluated the effects of BTE and dBTE solutions on the immortalized human chondrocyte cell line C-28/I2 (Merck, SCC043).[43,44] The cells were thawed from liquid nitrogen and maintained in Dulbecco's modified Eagle's medium (DMEM) high glucose (SIAL-DMEM-12-A), supplemented with 10% fetal bovine serum (FBS) (YOURSIAL-FBS-SA) and 1% penicillin–streptomycin (Gibco, 15140122) – hereafter referred to as complete culture medium – with medium changes every three days. Cell cultures were maintained at 37 °C in a humidified incubator with 5% CO_2.

2.5. Preparation of nutraceutical solutions

BTE and dBTE working solutions were prepared by diluting the stock solution (100 mg of nutraceutical resuspended in 1 mL of dimethyl sulfoxide, DMSO) in complete culture medium. To evaluate safety and biological effects, a concentration range of 5–50 μg mL^{-1} was selected based on previously reported bioactivity of *Curcuma caesia* extracts and other polyphenol-rich matrices in cellular models.[40]

2.6. Pro-inflammatory stimulation

C-28/I2 cells were seeded in 96-well plates at a density of 5000 cells per well in a complete culture medium and allowed to adhere to the plastic support for 24 h. Subsequently, 10 or 100 ng mL^{-1} IL-1β (Cell Guidance System, Aurogene, Rome, Italy), freshly prepared in complete culture medium, was added to the cells. C-28/I2 were then incubated for an additional 24 h. IL-1β concentrations were selected according to the experimental endpoint. A higher concentration was used for the wound healing assay to achieve a reproducible inhibition of cell migration, whereas a lower concentration was employed for the other assays to induce inflammation without causing excessive cellular stress. The concentrations were chosen based on previous reports and preliminary optimization experiments.

2.7. Determination of cell viability (MTT assay)

C-28/I2 cell viability was evaluated using the 3-(4,5-dimethylthiazol-2-yl)-2,5-diphenyltetrazolium bromide (MTT) assay. To evaluate the safety profile of BTE and dBTE, C-28/I2 cells were treated with increasing concentrations of the extract, ranging from 5 to 50 μg mL^{-1}, and cell viability was determined after 48 h of incubation. C-28/I2 cells were plated at a density of 5000 per well in 96-well plates and incubated for 24 h at 37 °C in a humidified 5% CO_2 incubator. Next, the cells were serum-starved for an additional 24 h before being treated with BTE and dBTE. Alternatively, to evaluate the chondroprotective potential, C-28/I2 cells were pre-treated with BTE and dBTE for 48 h before IL-1β treatment. Finally, 0.5 mg mL^{-1} of MTT reagent (Sigma-Aldrich, 475989-1GM) was added to the cells for 2 h at 37 °C. The resulting purple formazan crystals were solubilized using dimethyl sulfoxide (DMSO), and absorbance was measured at 570 nm using a

Table 2 Dynamic-MRM transitions, retention times, and optimized HPLC-ESI-MS/MS conditions for the targeted quantification of 38 phenolic markers

No.	Compounds	Precursor ion, *m/z*	Product ion, *m/z*	Fragmentor, V	Collision energy, V	Polarity	Retention time (R_t, min)	Delta retention time (ΔR_t)
1	Gallic acid	169	125.2[a]	97	12	Negative	6.96	2
2	Neochlorogenic acid	353	191.2[a], 179	82	12, 12	Negative	9.52	2
3	Delphindin-3-galactoside	465.01	303[a]	121	20	Positive	11.36	2
4	(+)-Catechin	289	245.2[a], 109.2	131	8, 20	Negative	11.44	2
5	Procyanidin B2	576.99	576.99[a], 321.2	160	0, 32	Negative	12.41	2
6	Chlorogenic acid	353	191.2[a], 127.5	82	12, 20	Negative	12.42	2
7	*p*-Hydroxybenzoic acid	137	93.2[a]	92	16	Negative	12.86	2
8	(−)-Epicatechin	289	245.1[a], 109.1	126	8, 20	Negative	13.03	2
9	Cyanidin-3-glucoside	449	287.3[a], 255.6	121	20, 20	Positive	13.14	2
10	Petunidin-3-glucoside	479.01	317[a], 302	121	20, 44	Positive	13.26	2
11	3-Hydroxybenzoic acid	137	93.2[a]	88	8	Negative	13.59	2
12	Caffeic acid	179	135.2[a], 134.1	92	12, 24	Negative	13.65	2
13	Vanillic acid	167	152.4[a], 108.1	88	12, 20	Negative	14.32	2
14	Resveratrol	227	185[a]	131	12	Negative	14.40	2
15	Pelargonidin-3-glucoside	433.01	271[a], 121	116	24, 50	Positive	14.52	2
16	Pelagonidin-3-rutinoside	579.01	271[a]	145	32	Positive	14.56	2
17	Malvidin-3-galactoside	493.01	331[a], 315.1	121	20, 50	Positive	14.64	2
18	Syringic acid	196.9	182.2[a], 121.2	93	8, 12	Negative	15.28	2
19	Procyanidin A2	575	575[a], 285	170	0, 20	Negative	16.18	2
20	*p*-Coumaric acid	163	119.2[a], 93.2	83	12, 36	Negative	16.70	2
21	Ferulic acid	193	134.2[a], 131.6	83	12, 8	Negative	17.10	2
22	3,5-Dicaffeoylquinic acid	514.9	353.1[a], 191	117	8, 28	Negative	17.61	2
23	Rutin	609	300.2[a], 271.2	170	32, 50	Negative	17.73	2
24	Hyperoside	465.01	303[a], 61.1	97	8, 50	Positive	18.33	2
25	Isoquercitrin	463	271.2[a], 300.2	155	44, 24	Negative	18.36	2
26	Delphindin-3,5-diglucoside	462.9	300.1[a]	165	24	Negative	18.38	2
27	Phloridzin	435.39	273[a], 167	155	8, 28	Negative	18.83	2
28	Quercitrin	446.99	300.2[a], 301.2	160	24, 16	Negative	19.61	2
29	Myricetin	316.99	179.1[a], 182	150	16, 24	Negative	19.61	2
30	Naringin	578.99	271.3[a], 151.3	170	32, 44	Negative	19.62	2
31	Kaempferol-3-glucoside	447	284.2[a], 255.2	170	24, 40	Negative	19.77	2
32	Hesperidin	611.01	303[a], 334.8	112	20, 12	Positive	20.19	2
33	Ellagic acid	301	301[a], 229	170	0, 24	Negative	21.41	2
34	*trans*-Cinnamic acid	149	131.2	74	4	Positive	21.44	2
35	Quercetin	300.99	151.2[a], 179.2	145	16, 12	Negative	21.87	2
36	Phloretin	272.99	167[a], 123	116	8, 20	Negative	22.30	2
37	Kaempferol	287.01	153[a], 69.1	60	36, 50	Positive	23.84	2
38	Isorhamnetin	314.99	300.2[a], 196.1	145	16, 4	Negative	24.57	2

[a] These product ions were used for quantification.

microplate reader (TECAN Infinite® M200 PRO). Cell viability was expressed as a percentage relative to untreated controls.

2.8. Wound healing assay

C-28/I2 cells were seeded in 6-well plates and treated with BTE and dBTE either alone for 48 h or as a pre-treatment before IL-1β exposure. The cells were incubated at 37 °C in a humidified atmosphere containing 5% CO_2 and cultured until reaching confluence to form monolayers. Subsequently, a linear mechanical wound was introduced along the horizontal axis of each well using the sterile tip of a pipette. Following scratching, the medium was removed, the cells were washed with Phosphate Buffered Saline (PBS) and then incubated for 24 h in fresh medium with or without IL-1β (100 ng mL^{-1}). Untreated cells served as the control group. Micrographs of the lesion areas were acquired immediately after scratching (T0) or after 24 h using a phase-contrast microscope (Olympus IX51 4× objective). Wound closure was quantified using ImageJ software (version 1.52a) by measuring the total area of the wound region. The percentage of wound closure was calculated according to the formula: Wound closure (%) = [(original wound gap − remaining wound gap)/original wound gap] × 100.[45]

2.9. Quantification of TNF-α release

The levels of secreted TNF-α in cell culture supernatants were measured using the Human TNF-alpha DuoSet ELISA kit,

according to the manufacturer's instructions. Supernatants were collected after 48 h of treatment with BTE or dBTE, either alone or as a pre-treatment before a 24 h stimulation with 10 ng mL^{-1} IL-1β. Afterwards, the cells underwent a 24 h recovery period, and were finally analyzed using the TNF-α ELISA kit (DY210, R&D Systems, Minneapolis, MN, USA).

2.10. Transmission electron microscopy (TEM)

Control and treated cells were washed and fixed with 2.5% glutaraldehyde in 0.1 M phosphate buffer (pH 7.3) for 15 min. The cells were then scraped and centrifuged at 300*g* for 10 min, and the pellets were fixed in 2.5% glutaraldehyde for an additional 30 min. The samples were post-fixed in 1% osmium tetroxide (OsO_4) for 1 h, alcohol dehydrated and embedded in araldite. For ultrastructural analysis, thin sections were stained with UranyLess and lead citrate and analyzed using a Philips CM10 transmission electron microscope (FEI Italia SRL, Milano, Italy). Mitochondrial density and cristae number were evaluated using the microscope software. Mitochondrial size was assessed by analyzing 10 areas of 20 μm^2 for experimental condition. Mitochondrial density was quantified in 10 cells for experimental condition, whereas cristae number was determined by analyzing 15 mitochondria for cell. All measurements were performed under identical imaging and analysis conditions.

2.11. Confocal laser scanning microscopy (CLSM)

To obtain high-resolution fluorescence images of treatment-induced changes, confocal microscopy was performed. Chondrocytes were grown on 18 × 18 mm coverslips placed in 24-well plates and subjected to pre-treatment with 10 μg BTE and dBTE for 48 h. Inflammation was then induced using 10 ng mL^{-1} IL-1β for 24 h. Following treatments, the cells were fixed with 4% paraformaldehyde (PFA) prepared in 1× PBS.

2.11.1. Evaluation of $\Delta\Psi_m$ by JC-1 staining. Control and treated C-28/I2 cells were exposed to the JC-1 probe to evaluate the functionality of mitochondrial membrane potential ($\Delta\Psi_m$). Chondrocytes were exposed to JC-1 probe (ab288313, Abcam) for 20 min at 37 °C. Samples were observed through a Leica TCS-SP5 Confocal connected to a DMI 6000 CS Inverted Microscope (Leica Microsystems CMS GmbH; objectives 40× and 60×); excitation was set at 488 nm fluorescein isotiocianato (FITC), and emission signals were detected at 525 nm (JC-1). CLSM images are presented as single-plane images or Z-stack projections.

2.11.2. Evaluation of the mitochondrial mass by NAO staining. To assess the mitochondrial mass in untreated and treated C-28/I2 cells, fresh cell pellets were exposed to the fluorescent probe 10-nonyl acridine orange (NAO). Briefly, 50 nM NAO (A7847, Sigma-Aldrich) was added to each sample for 10 min at room temperature (RT); the specimens were then rinsed in PBS and finally observed through a CLSM. Excitation and emission signals were 488 nm and 519 nm for NAO. Densitometric analysis of NAO immunofluorescence was performed using ImageJ software (version 1.54j, National Institutes of Health, Bethesda, MD, USA) on 10 images per experimental condition. Fluorescence intensity was quantified within a standardized square region of interest (ROI) measuring 250 × 250 μm in each image. All images were acquired using identical microscope settings and analyzed under the same conditions. Images were collected at the same magnification, with a 50 μm scale bar.

2.11.3. Nrf2 immunostaining. To assess the expression and localization of nuclear factor erythroid 2-related factor 2 (Nrf2), an immunofluorescence assay was performed. After fixation, cells were incubated overnight with a polyclonal rabbit anti-Nrf2 antibody (AC-A95354-100, SIAL) at a 1 : 100 dilution in a mixture of PBS, 2% bovine serum albumin (BSA), and 5% normal goat serum (NGS) to block nonspecific binding. Following primary antibody incubation, cells were washed with PBS and incubated for 2 h with a goat anti-rabbit IgG secondary antibody conjugated with a fluorophore (A-11008, ThermoFisher Scientific) at a 1 : 400 dilution in PBS, BSA 2%, and NGS 5%. After staining, coverslips were mounted onto slides using an anti-fade mounting medium, Vectashield H-100 (H-1000-10, Vector Laboratories), and fluorescence signals were visualized using a Leica TCS-SP5 Confocal Microscope connected to a DMI 6000 CS Inverted Microscope.

2.11.4. NLR family pyrin domain containing 3 (NLRP3) immunostaining. To evaluate the expression and localization of NLRP3 (NOD-, LRR- and pyrin domain-containing protein 3), a key component of the innate immune system that forms the NLRP3 inflammasome, an immunofluorescence assay was performed. After fixation, cells were incubated overnight with a polyclonal rabbit anti-NLRP3 antibody (A14882, SIAL) at a 1 : 100 dilution in a mixture of PBS, 2% BSA, and 5% NGS to block nonspecific binding. Following primary antibody incubation, cells were washed with PBS and incubated for 2 h with a goat anti-rabbit IgG secondary antibody conjugated with a fluorescein (AP132F, Millipore) at a 1 : 200 dilution in PBS, BSA 2%, and NGS 5%. After staining, coverslips were mounted onto slides using an anti-fade mounting medium, Vectashield H-100 (H-1000-10, Vector Laboratories), and fluorescence signals were visualized using a Leica TCS-SP5 Confocal Microscope connected to a DMI 6000 CS Inverted Microscope. Densitometric analysis of NLRP3 immunofluorescence was performed using ImageJ software (version 1.54j, National Institutes of Health, Bethesda, MD, USA) on 11 images per experimental condition. Fluorescence intensity was quantified within a standardized square region of interest (ROI) measuring 250 × 250 μm in each image. All images were acquired using identical microscope settings and analyzed under the same conditions. Images were collected at the same magnification, with a 50 μm scale bar.

2.12. Statistical analysis

For MTT assays, one-way Analysis of Variance (ANOVA) was performed to compare between-groups variance and within-group variance, followed by Šídák's multiple comparison test to identify specific groups with statistically significant differences. Data are expressed as mean ± standard deviation (SD) from at least three independent experiments. Data obtained from wound-healing and ELISA assays were analyzed using

two-way ANOVA followed by Tukey's multiple comparison test and are presented as mean ± SD from at least four and three independent experiments, respectively. Quantification of mitochondrial size is reported as mean ± SD of four measurements across three different fractions, whereas cristae number is presented as mean ± SD from ten cells per condition across three different fractions. These datasets were analyzed using two-way ANOVA followed by Tukey's multiple comparison test. NAO fluorescence intensity was quantified as Mean Fluorescence Intensity (MFI, %) and is expressed as mean ± SD from at least ten distinct, non-overlapping fields per condition; two-way ANOVA was performed, followed by Tukey's multiple comparison test. NLRP3 fluorescence intensity was quantified as MFI and is expressed as mean ± SD from eleven distinct, non-overlapping fields per condition; two-way ANOVA was performed, followed by Šídák's multiple comparison test. For all analyses, the threshold for statistical significance was set at $P < 0.05$, and significance levels were assigned as follows: *P value <0.05, **$P < 0.01$, ***$P < 0.001$, ****$P < 0.0001$. Statistical analyses were conducted using GraphPad Prism software.

3. Results

3.1. Stability of BTE phenolic compounds during *in vitro* gastrointestinal digestion

As shown in Table 3, the recovery of phenolic compounds was generally reduced following the digestive process. This was particularly evident for flavan-3-ols – including catechin (C), epicatechin (EC), and procyanidin B2 (PB2) – whose concentrations decreased from 345.52 to 45.12 mg kg^{-1}, from 695.34 to 268.97 mg kg^{-1}, and from 346.52 to 163.70 mg kg^{-1}, respectively. Conversely, the recovery of other polyphenol classes, such as phenolic acids, was less affected by digestion. HPLC-MS/MS analysis revealed comparable levels of some hydroxybenzoic and hydroxycinnamic acids before and after simulated digestion. Among the most abundant compounds, 4-hydroxy benzoic acid (4-HBA) and syringic acid (SA) showed stable levels (233.31 *vs.* 222.84 mg kg^{-1} and 198.36 *vs.* 189.70 mg kg^{-1}, respectively), whereas 3-hydroxy benzoic acid (3-HBA) and vanillic acid (VA) exhibited reduced, yet still relatively high, concentrations (478.62 *vs.* 355.80 and 416.91 *vs.* 315.35 mg kg^{-1}, respectively). By contrast, *p*-coumaric acid (*p*-CA) and ferulic acid (FA) levels were markedly reduced by gastrointestinal digestion (211.80 *vs.* 86.70 and 174.04 *vs.* 55.22 mg kg^{-1}, respectively). Regarding flavonols, although overall detected at lower amounts in BTE, their concentrations were only partially impacted by the digestive process. Altogether, these results highlight the compound-dependent stability of the BTE phenolic fraction, comprising both highly stable and less bioaccessible phytochemicals.

Table 3 Quantitative profile of phenolic compounds (mg per kg dry weight of the freeze-dried extract) in blue turmeric extract before and after simulated gastrointestinal digestion (BTE *vs.* dBTE)

No.	Compound	BTE (mg kg^{-1})	dBTE (mg kg^{-1})
1	Gallic acid	80.87	55.64
2	Neochlorogenic acid	22.21	18.62
3	Delphinidin 3-galactoside	n.d.	5.84
4	Catechin	345.52	45.12
5	Procyanidin B2	346.52	163.70
6	Chlorogenic acid	55.12	54.22
7	4-Hydroxy benzoic acid	233.31	222.84
8	Epicatechin	695.34	268.97
9	3-Hydroxy benzoic acid	478.62	355.80
10	Caffeic acid	18.91	14.27
11	Vanillic acid	416.91	315.35
12	Syringic acid	198.36	189.70
13	Procyanidin A2	50.12	56.88
14	P-Coumaric acid	211.80	86.70
15	Ferulic acid	174.04	55.22
16	3,5-Dicaffeoylquinic acid	88.32	79.24
17	Rutin	23.27	17.50
18	Isoquercitrin	10.05	11.87
19	Delphinidin 3,5-diglucoside	19.93	7.26
20	Kaempferol 3-glucoside	n.d.	n.d.
21	Ellagic acid	36.16	28.69
22	Quercetin	16.57	n.d.
23	Isorhamnetin	1.09	n.d.

3.2. Assessment of C-28/I2 cell viability upon BTE exposure

To exclude potential cytotoxic activities of BTE, C-28/I2 metabolic activity was evaluated after 48 h treatments with BTE at a concentration range of 5–50 μg mL^{-1} using the MTT assay. Notably, C-28/I2 metabolic activity remained unaffected at all tested concentrations, with values comparable to those of the untreated control groups (Fig. 1A). Similarly, cell viability was not affected by the BTE bioaccessible fraction (dBTE), as no metabolic alterations were detected after 48 h of treatment with increasing concentrations (5–50 μg mL^{-1}) of dBTE (Fig. 1B). Altogether, these results suggest the safety profile of BTE in human chondrocytes.

3.3. Cell viability evaluation in BTE-treated C-28/I2 exposed to IL-1β

To assess BTE protection against IL-1β-induced cytotoxicity, cell viability was measured in C-28/I2 cells pre-treated with BTE and dBTE prior to IL-1β stimulation. As expected, IL-1β treatment exerted cytotoxic effects, resulting in an approximately 30% reduction in cell viability compared to untreated controls. Conversely, a 48 h pre-treatment with BTE prevented IL-1β-induced cytotoxicity at all tested concentrations (5–50 μg mL^{-1}). As shown in Fig. 2, the protective effects of BTE were retained following *in vitro* gastrointestinal digestion; IL-1β-exposed cells pre-treated with dBTE maintained viability levels comparable to those of untreated cells, demonstrating that the chondroprotective activity of BTE is preserved within the bioaccessible fraction of phytochemicals soluble in the digestive fluids.

3.4. Evaluation of C-28/I2 wound healing capacity

The wound healing capacity of C-28/I2 cells was assessed using the scratch assay under baseline conditions, following IL-1β exposure, and after treatment with BTE, either alone or as a pre-treatment prior to IL-1β stimulation (Fig. 3A). As shown in Fig. 3B, a 48 h treatment with BTE at both 5 and 10 μg mL^{-1} significantly enhanced migratory capacity, resulting in an approximately 15%

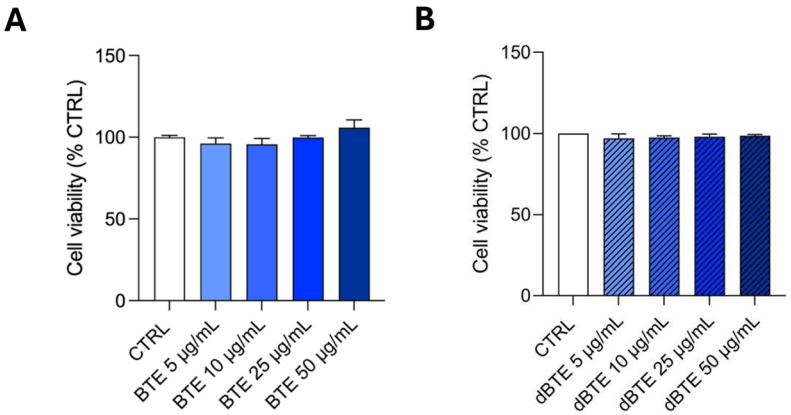

Fig. 1 Evaluation of C-28/I2 viability upon BTE treatments. Viability of C-28/I2 cells after 48 h treatments with varying concentrations (5–50 µg mL^{-1}) of BTE (A) and dBTE (B). MTT data are expressed as absorbance at 570 nm and normalized to untreated controls (% CTRL). Data are presented as mean ± SD from at least three independent experiments.

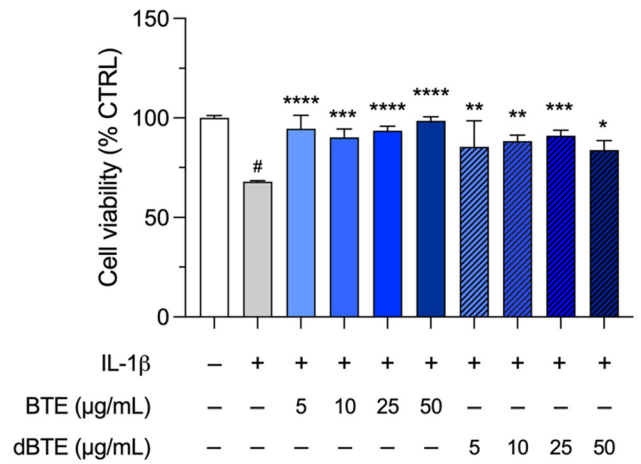

Fig. 2 Assessment of BTE and dBTE protective effects on cell viability in C-28/I2 cells exposed to IL-1β. C-28/I2 cell viability was evaluated in untreated and treated cells. Data from the MTT assay are expressed as absorbance at 570 nm and normalized to untreated controls (% CTRL). Data are presented as mean ± SD from three independent experiments. Ordinary one-way ANOVA, Šídák's multiple comparison test ($^{\#}P$ value < 0.0001 CTRL *vs.* IL-1β-treated cells. $^{*}P < 0.05$, $^{**}P < 0.01$, $^{***}P < 0.001$, $^{****}P < 0.0001$ IL-1β-treated cells *vs.* BTE and dBTE pre-treated cells).

increase in wound closure compared to untreated controls. Notably, this effect was maintained in dBTE-treated C-28/I2 cells, whose migratory capacity similarly improved at both 10 and 50 µg mL^{-1} (Fig. 3C). Conversely, IL-1β stimulation only marginally affected C-28/I2 migratory capacity and did not influence the response to either BTE or dBTE (SI Tables S1 and S2). Overall, these results underscore the regenerating potential of the BTE bioaccessible fraction, which is not impacted by IL-1β.

3.5. Evaluation of TNF-α release in BTE-treated C-28/I2 exposed to IL-1β

The release of the inflammatory mediator TNF-α from C-28/I2 cells was measured by ELISA under baseline conditions, following IL-1β exposure, and after treatment with BTE, either alone or as a pre-treatment prior to IL-1β stimulation. IL-1β-exposed C-28/I2 cells showed a marked increase in TNF-α release compared to untreated controls. In contrast, a 48 h treatment with BTE at both 5 and 10 µg mL^{-1} effectively prevented IL-1β-induced TNF-α secretion. Notably, this activity was maintained in C-28/I2 cells treated with the bioaccessible fraction of BTE (dBTE), further reflecting a protective role of this phytocomplex in inflamed chondrocytes (Fig. 4).

3.6. Ultrastructural analysis of BTE-treated C-28/I2 stimulated with IL-1β

TEM ultrastructural analyses were employed to evaluate morphological changes in the cellular membrane, nucleus, and intracytoplasmic organelles under baseline conditions, IL-1β stimulation, and BTE pre-treatment. As shown in Fig. 5, untreated and BTE-treated C-28/I2 cells displayed similar morphological features. Under these experimental conditions, the cells appeared elongated, with numerous well-preserved mitochondria, abundant endoplasmic reticulum, and a conserved nucleus characterized by an intact double membrane and diffuse chromatin (Fig. 5A–C). Following IL-1β exposure, numerous small and large empty vacuoles emerged, accompanied by the formation of autophagic vacuoles. Moreover, the phospholipid bilayer appeared detached, and several mitochondria were empty and damaged (Fig. 5D–G). Conversely, pre-treatments with BTE and its bioaccessible fraction dBTE effectively preserved nuclear and cytoplasmic ultrastructure, as well as mitochondrial and endoplasmic reticulum morphology (Fig. 5H–J).

3.7. Morphometric analysis of BTE-treated C-28/I2 stimulated with IL-1β

Mitochondrial ultrastructure of C-28/I2 cells was evaluated by morphometric analysis. In untreated, BTE-, and dBTE-treated cells, mitochondria displayed well-preserved outer membranes and cristae. Across these conditions, mitochondrial diameters, ranging between 550 and 600 nm, and cristae number were

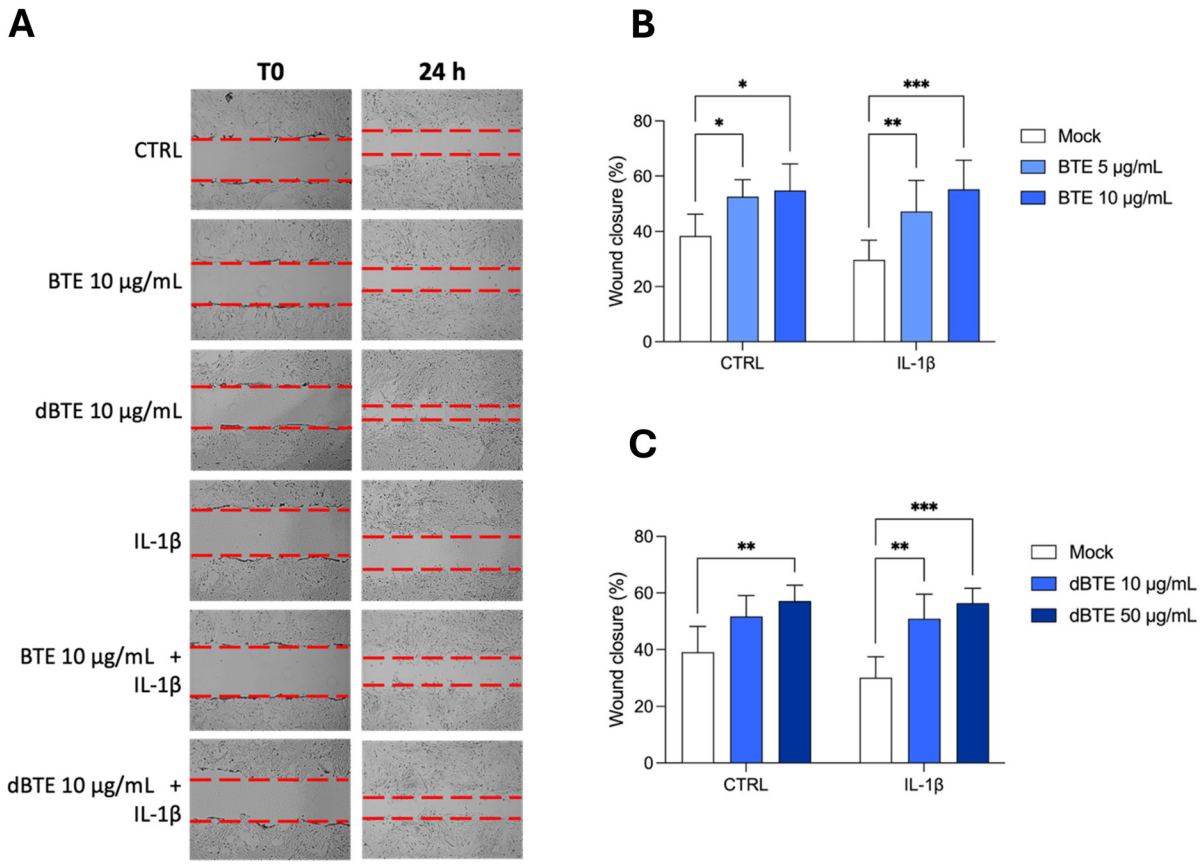

Fig. 3 Evaluation of C-28/I2 migratory capacity upon BTE and dBTE treatments. The migratory capacity of C-28/I2 cells was evaluated in untreated and treated groups. Exposure to IL-1β was performed after 48 h pre-treatments with BTE or dBTE (panels B and C). Representative images at time 0 (T0) and after 24 h (24 h) are shown in panel A. Data are presented as mean ± SD from at least four independent experiments, each performed in triplicate. Ordinary two-way ANOVA, Tukey's multiple comparison test, *P value <0.05, **P < 0.01, ***P < 0.001, ****P < 0.0001.

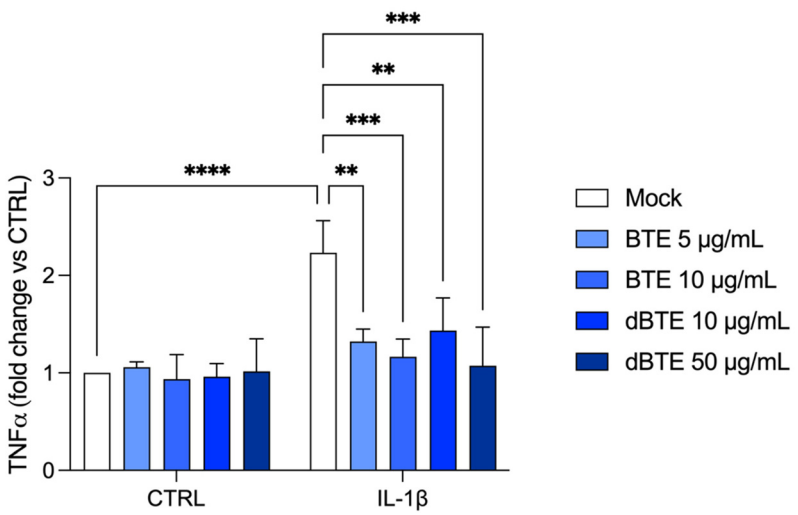

Fig. 4 Evaluation of BTE and dBTE protective effects on TNF-α release in C-28/I2 cells under IL-1β exposure. The release of TNF-α from C-28/I2 cells was measured by ELISA in untreated and treated cells. Data are presented as mean ± SD from three independent experiments. Ordinary two-way ANOVA, Tukey's multiple comparison test, *P value <0.05, **P < 0.01, ***P < 0.001, ****P < 0.0001.

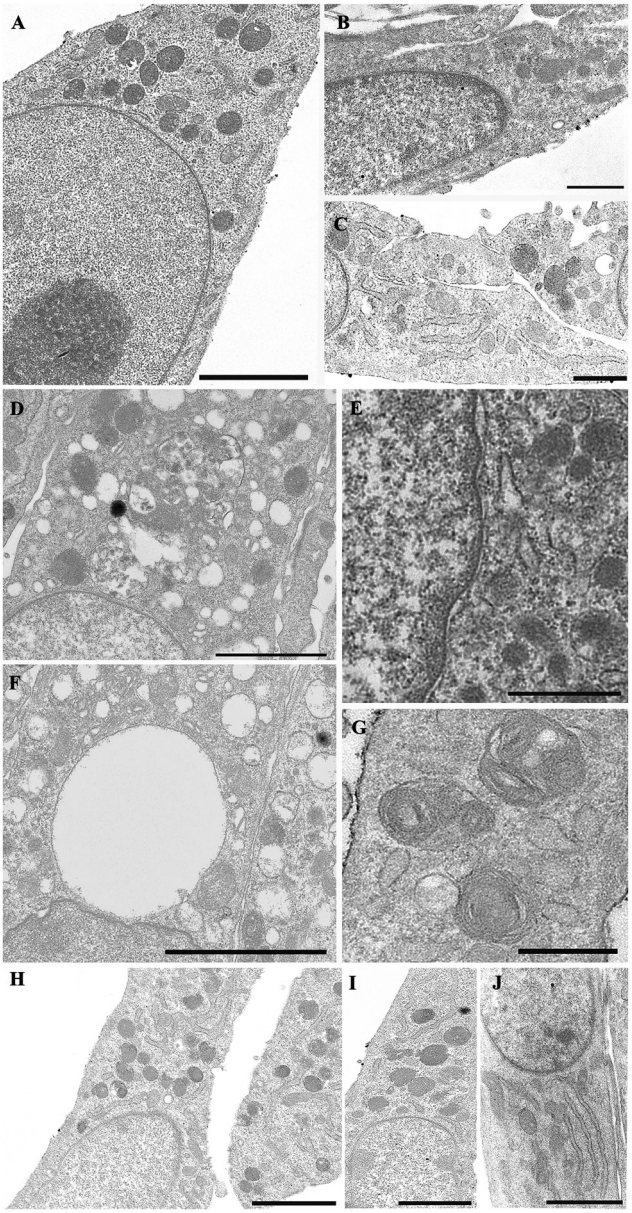

Fig. 5 Ultrastructural analysis of C-28/I2 cells under different conditions. TEM analysis of C-28/I2 cell morphology under different conditions: untreated controls (A), BTE- and dBTE-treated cells (B and C), IL-1β-exposed cells (D–G), and IL-1β-exposed cells pre-treated with BTE or dBTE (H–J). IL-1β treatments were performed at 10 ng mL^{-1} for 24 h. BTE and dBTE treatments were performed at 10 μg mL^{-1} for 48 h. Scale bar: 1 μm.

comparable (Fig. 6A–C). Conversely, in IL-1β-stimulated cells, mitochondria appeared flattened, emptied, smaller in size (350–380 nm), and characterized by a reduced number of cristae (Fig. 6D). Notably, in cells pre-treated with BTE and dBTE, mitochondrial morphology was preserved, with dimensions (520–550 nm) and cristae distribution comparable to those of untreated cells (Fig. 6E and F). Overall, these results support the preservation of mitochondrial integrity mediated by BTE under IL-1β-driven inflammatory conditions.

3.8. Evaluation of the mitochondrial mass and $\Delta\Psi_m$ in BTE-treated C-28/I2 exposed to IL-1β

To further investigate the mitoprotective activity of BTE against IL-1β-induced damage, the mitochondrial mass and $\Delta\Psi_m$ were assessed through CLSM analysis using NAO and JC-1 staining. In viable cells characterized by high $\Delta\Psi_m$, JC-1 accumulates as aggregates emitting orange-red fluorescence. Accordingly, untreated and BTE-treated C-28/I2 cells exhibited JC-1 red fluorescence, indicating preserved $\Delta\Psi_m$ (Fig. 7A–C). Conversely, in damaged cells characterized by low $\Delta\Psi_m$, JC-1 exists as monomers emitting green fluorescence. Under IL-1β stimulation, JC-1-associated green fluorescence indicated impaired $\Delta\Psi_m$ (Fig. 7D). Notably, pre-treatment with BTE and dBTE preserved JC-1-associated red fluorescence, indicating preservation of mitochondrial function (Fig. 7E and F). To evaluate mitochondrial integrity, NAO-associated fluorescence was measured in C-28/I2 cells under different conditions. NAO dye emits green fluorescence upon binding cardiolipin and accumulates in intact mitochondria. In cells treated with BTE and dBTE, NAO fluorescence was comparable to control conditions (Fig. 8A–C). Conversely, exposure to IL-1β markedly reduced NAO signals, indicating mitochondrial damage (Fig. 8D). NAO fluorescence was preserved in IL-1β-stimulated cells pre-treated for 48 h with both BTE and its bioaccessible fraction dBTE (Fig. 8E and F). This effect was further confirmed by quantitative analysis of NAO signals, which were significantly reduced upon IL-1β exposure but partially preserved in cells pre-treated with BTE and dBTE (Fig. 8G). Altogether, these results are consistent with a mitoprotective activity of BTE in inflamed chondrocytes.

3.9. Assessment of Nrf2 activation in BTE-treated C-28/I2 exposed to IL-1β

BTE antioxidant potential was investigated by assessing Nrf2 localization in C-28/I2 cells under control conditions and following IL-1β exposure, either alone or following pre-treatment with BTE. In control, BTE-, and dBTE-treated cells, Nrf2 was mainly localized in the cytoplasmic compartment, accumulating as a predominantly inactive pool (Fig. 9A–C). Upon IL-1β stimulation, Nrf2-related signals were mainly detected in the nuclear compartment, indicating Nrf2 translocation to the nucleus and transcriptional activation of antioxidant genes (Fig. 9D). Notably, pre-treatment with BTE and dBTE prevented Nrf2 nuclear translocation in inflamed chondrocytes, supporting the redox-regulating activities of BTE under conditions of IL-1β-induced cellular stress (Fig. 9E and F). Nrf2 is a key regulator of the cellular antioxidant response, and its nuclear translocation is generally regarded as an adaptive mechanism activated under oxidative stress. Therefore, the reduced Nrf2 nuclear localization observed following BTE and dBTE treatment should not be interpreted as a direct inhibition of this protective pathway. Rather, it may reflect a reduced requirement for Nrf2 activation because of the attenuation of IL-1β-induced oxidative stress. This interpretation is consistent with the overall decrease in inflammatory and oxidative stress-related markers observed in treated cells.

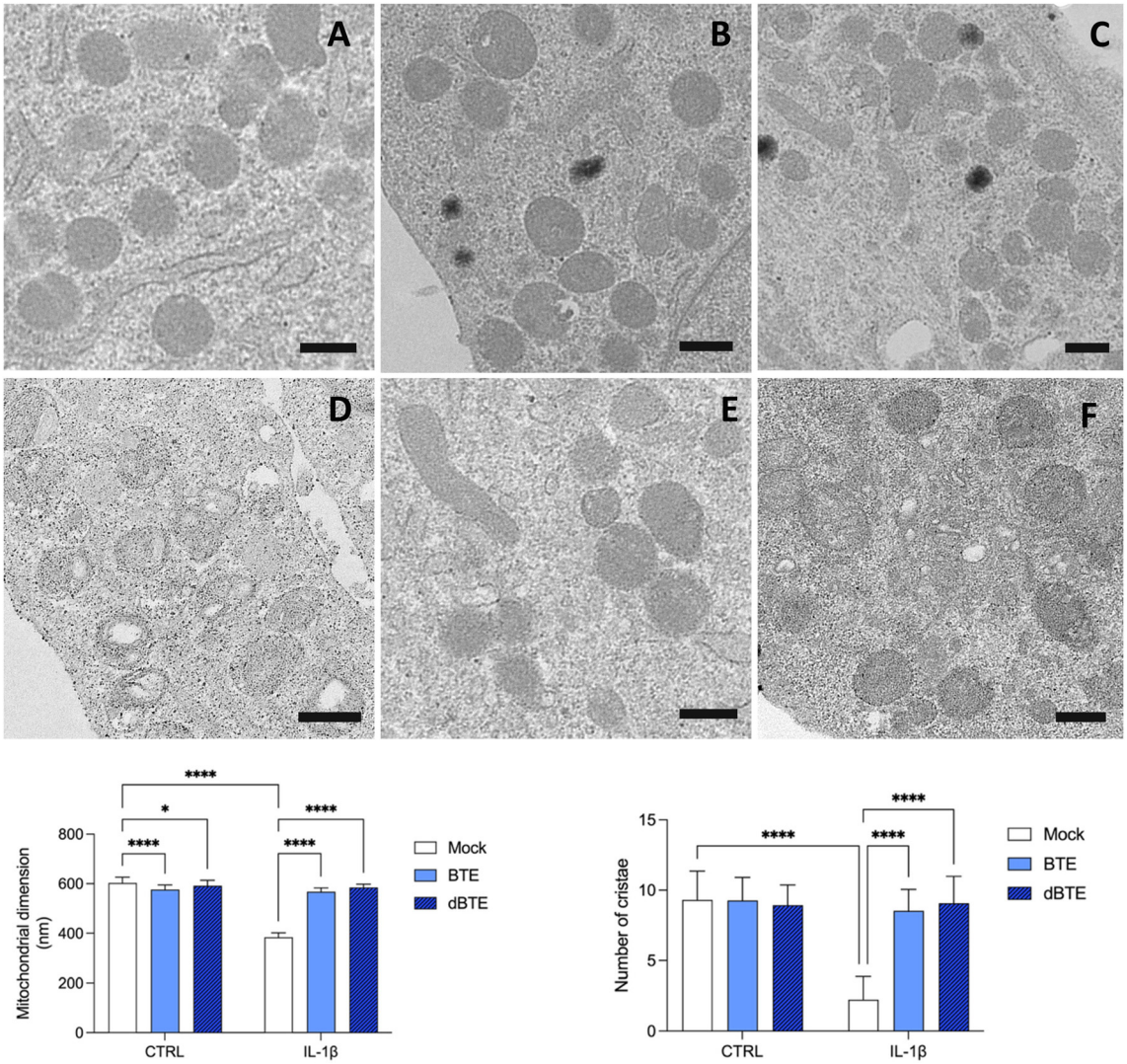

Fig. 6 Morphometric analysis of mitochondria in C-28/I2 cells under different conditions. TEM analysis of mitochondrial morphology in C-28/I2 cells under different conditions: untreated controls (A), BTE- and dBTE-treated cells (B and C), IL-1β-exposed cells (D), and IL-1β-exposed cells pre-treated with BTE or dBTE (E and F). IL-1β treatments were performed at 10 ng mL^{-1} for 24 h. BTE and dBTE treatments were performed at 10 μg mL^{-1} for 48 h. Scale bar: 500 nm. Quantification of mitochondrial size and cristae number under baseline conditions and following treatment is shown in the bottom panels. Mitochondrial size is expressed as mean ± SD of four measurements across three different fractions (bottom, left). Cristae number is presented as mean ± SD from ten cells per condition across three different fractions (bottom, right). Ordinary two-way ANOVA, Tukey's multiple comparison test, *P value < 0.05, **P < 0.01, ***P < 0.001, ****P < 0.0001.

3.10. Assessment of NLRP3 activation in BTE-treated C-28/I2 exposed to IL-1β

The anti-inflammatory potential of BTE was investigated by assessing NLRP3 localization in C-28/I2 cells under control conditions and following IL-1β exposure, either alone or following pre-treatment with BTE. In control, BTE-, and dBTE-treated cells, NLRP3 appeared diffusely localized throughout the cytoplasm, and the fluorescence signal was weak (Fig. 10A–C). Upon IL-1β stimulation, NLRP3-related signals were predominantly detected in the perinuclear region, with enhanced fluorescence intensity and the appearance of puncta/speck aggregates (Fig. 10D and E). Notably, pre-treatment with both BTE and dBTE prevented the IL-1β-induced increase in NLRP3 fluorescence intensity and perinuclear localization, restoring a pattern comparable to control conditions (Fig. 10F and G). This protective activity was further confirmed by quantitative analysis of NLRP3 fluorescence signals, which were significantly enhanced upon IL-1β exposure but partially preserved in cells pre-treated with BTE and dBTE (Fig. 10H). Overall, these findings further support the role of BTE as an upstream modulator of inflammation.

4. Discussion

Emerging research increasingly highlights the potential of dietary polyphenols to act within a nutraceutical framework by

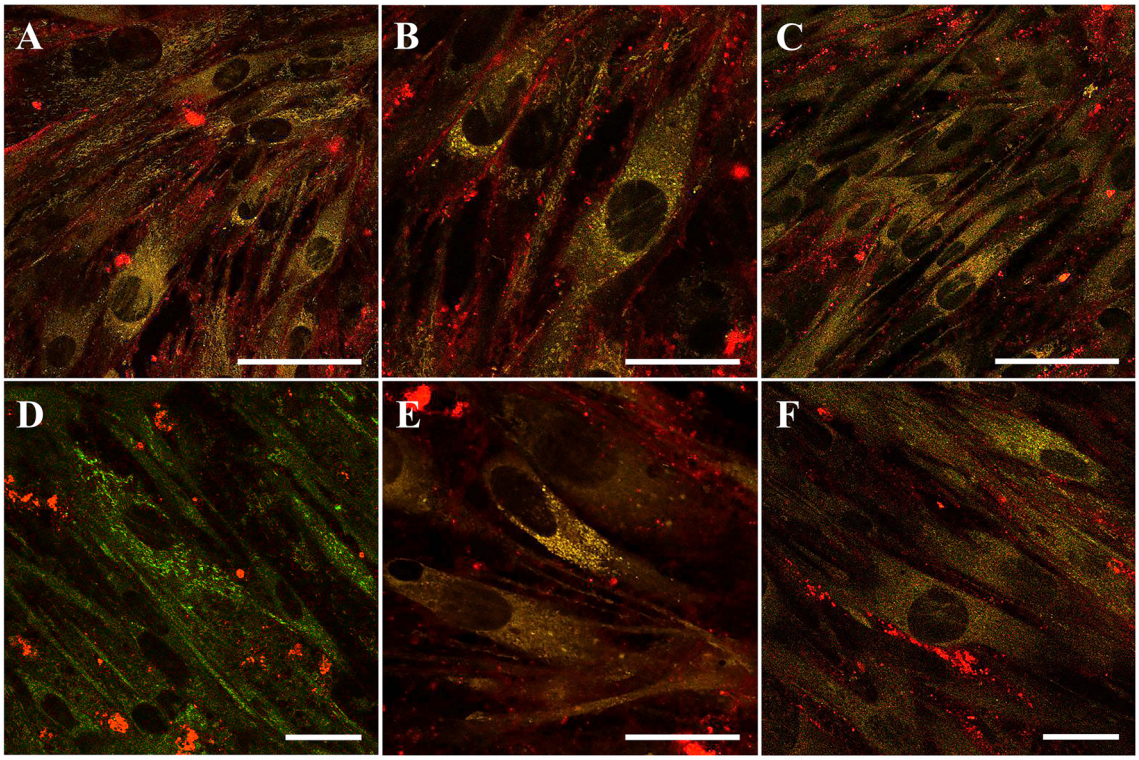

Fig. 7 Evaluation of $\Delta\Psi_m$ in C-28/I2 cells under different conditions. CLSM analysis of $\Delta\Psi_m$ in C-28/I2 cells using JC-1 staining under various conditions: untreated controls (A), BTE- and dBTE-treated cells (B and C), IL-1β-exposed cells (D), and IL-1β-exposed cells pre-treated with BTE or dBTE (E and F). Scale bar: 50 μm for A, C, D and F, 25 μm for B and E.

modulating inflammatory and oxidative pathways and supporting cartilage homeostasis, thereby contributing to the maintenance of joint health. Accordingly, polyphenol-rich nutraceuticals may be positioned within a "before drugs, beyond foods" framework aimed at supporting joint homeostasis.[18,46,47] Among these, *Curcuma caesia* Roxb. has emerged as a promising source of phenolics endowed with anti-inflammatory and antioxidant properties. In this study, we evaluated the phenolic profile and the biological effects of a *Curcuma caesia* Roxb. phytocomplex (BTE) and its bioaccessible fraction (dBTE) in inflamed human chondrocytes. Specifically, inflammatory marker release, mitochondrial function and integrity, antioxidant response activation, chondrocyte viability, and wound-healing capacity were evaluated under inflammatory conditions.[48] In this regard, cell culture-based antioxidant assays, including the assessment of Nrf2 activation, provide a biologically relevant system for evaluating antioxidant activity, complementing conventional chemical assays.[49] Our findings indicate that *Curcuma caesia* extracts mitigate inflammatory responses, as pre-treatment with both BTE and dBTE prevented IL-1β-induced TNF-α release and NLRP3 perinuclear localization. NLRP3 inflammasome activation can be triggered by several endogenous stimuli, including IL-1β and TNF-α.[50] By attenuating the TNF-α-NLRP3 signalling axis, *Curcuma caesia* Roxb. may act as a broad modulator of the inflammatory response. Moreover, BTE and dBTE partially prevented mitochondrial dysfunction while promoting the activation of antioxidant responses under inflammatory conditions. Phenotypically, BTE preserved chondrocyte viability under IL-1β-stimulation, and the regenerative potential of C-28/I2 was overall enhanced by both BTE and its bioaccessible fraction. Phytochemical analyses revealed a complex profile of bioactive compounds, with flavanols – including epicatechin, catechin, and procyanidin B2 – and phenolic acids – such as 3-hydroxybenzoic acid, 4-hydroxybenzoic acid, and vanillic acid – representing the most abundant subclasses. These compounds are known for their anti-inflammatory properties and ability to modulate key molecular pathways involved in OA. Epicatechin (EC), the most abundant flavanol, exhibits antioxidant and anti-inflammatory effects. It inhibits nuclear factor kappa-light-chain-enhancer of activated B cells (NF-κB) activation and reduces reactive oxygen species (ROS) production, thereby protecting chondrocytes from oxidative stress. These findings are consistent with previous studies in which EC, tested in Detroit 551 human fibroblast cells, substantially reduced Matrix Metalloproteinase-1 (MMP-1) activity at comparable concentrations. In the present study, the EC content within the phytocomplex was approximately 6.95 ng mL^{-1} at an effective extract concentration of 10 μg mL^{-1}. This suggests that the phytocomplex may contribute to anti-MMP-1 activity, even at relatively low levels of EC, potentially through synergistic interactions among its bioactive constituents. Procyanidin B2 (PB2), a key compound in the BTE extract, has been reported to inhibit both MMP expression and reduce the secretion of pro-inflam-

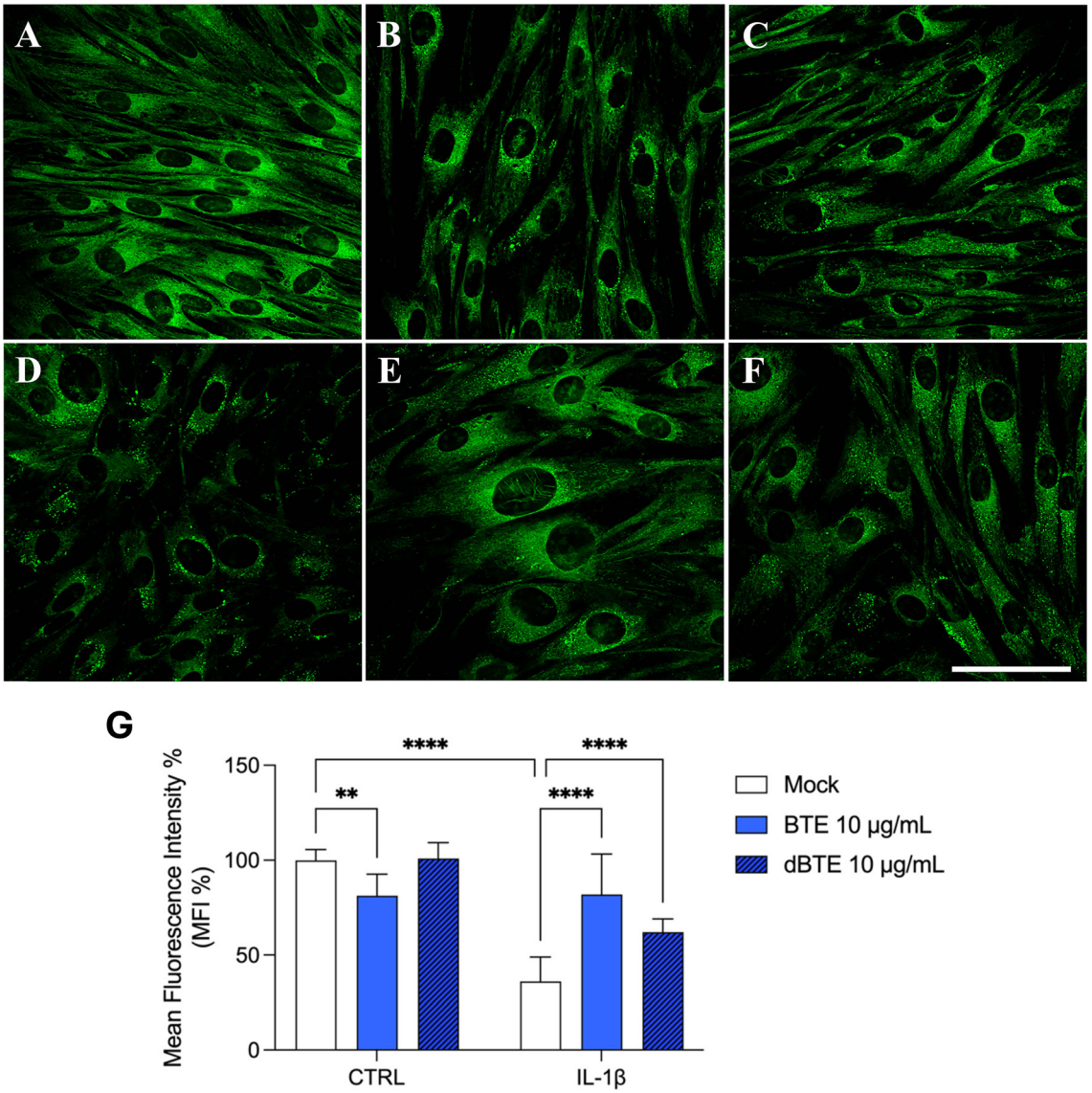

Fig. 8 Evaluation of the mitochondrial mass in C-28/I2 cells under different conditions. CLSM analysis of the mitochondrial mass in C-28/I2 cells using NAO staining under various conditions: untreated controls (A), BTE- and dBTE-treated cells (B and C), IL-1β-exposed cells (D), and IL-1β-exposed cells pre-treated with BTE or dBTE (E and F). Scale bar: 50 µm. Quantification of NAO fluorescence intensity is shown in panel G. Data are expressed as Mean Fluorescence Intensity (MFI, %), and the results are presented as mean ± SD from at least ten distinct, non-overlapping fields for each condition. Statistical analysis was performed using ordinary two-way ANOVA, Tukey's multiple comparison test, *P value <0.05, **P < 0.01, ***P < 0.001, ****P < 0.0001.

matory cytokines, including interleukin-6 (IL-6) and interleukin-8 (IL-8), in chondrocytes at a concentration of 20 µM (equivalent to 11.57 µg mL^{-1}).[51–53] In the present study, BTE exhibited anti-inflammatory effects at a total extract concentration of 10 µg mL^{-1}, corresponding to approximately 3.47 ng mL^{-1} PB2 (equivalent to 6 nM). This observation suggests that PB2, in combination with other bioactive constituents of the blend, may contribute to the observed anti-inflammatory activity. Furthermore, hydroxybenzoic acids may contribute to inflammation modulation and bone health maintenance. In particular, vanillic acid (VA) has been associated with anti-inflammatory activity in rat models of OA by targeting the NLRP3 inflammasome. In these models, VA administration (30 mg kg^{-1}) for 40 days markedly reduced pain-related behaviours and downregulated the levels of pro-inflammatory and pro-apoptotic markers.[54] Moreover, in *in vitro* OA models, pre-treatment with VA in a concentration range of 5–20 µg mL^{-1} reduced IL-1β-induced chondrocyte hypertrophy and attenuated inflammatory responses by interfering with MAPK and PI3K/AKT/NF-κB signalling pathways.[55] In our study, high levels of VA were detected in both BTE and its bioaccessible fraction, supporting a potential contribution of this compound to the overall behaviour of C-28/I2 chondrocytes. Notably, the VA content at the active BTE concentration range corresponds to approximately

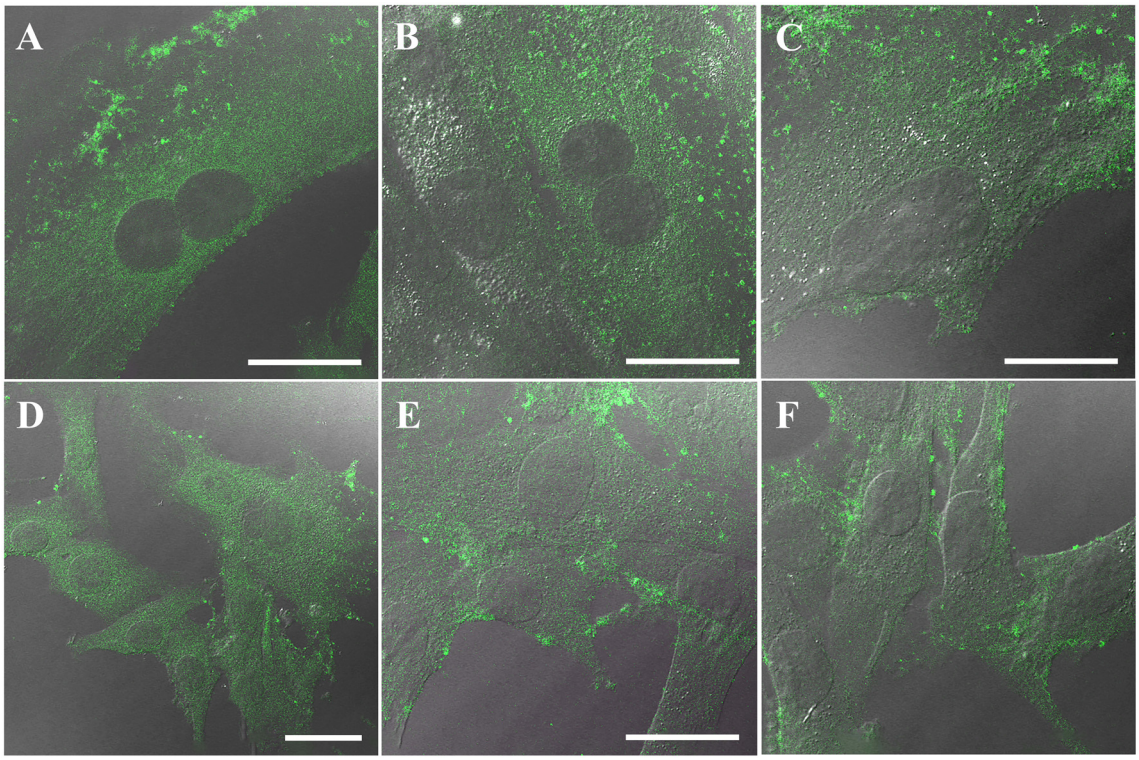

Fig. 9 Assessment of Nrf2 activation in C-28/I2 cells under different conditions. CLSM analysis of Nrf2 localization in C-28/I2 cells under various conditions: untreated controls (A), BTE- and dBTE-treated cells (B and C), IL-1β-exposed cells (D), and IL-1β-exposed cells pre-treated with BTE or dBTE (E and F). Scale bar: 25 μm for A, B, C, E and F, 50 μm for D.

4.17 ng mL^{-1}, suggesting that additional constituents and/or synergistic effects within the phytocomplex are likely involved in the overall functional activity. Likewise, 4-hydroxybenzoic acid (4-HBA) has been reported to exert chondroprotective effects in inflammatory OA models. In osteoarthritic chondrocytes, 4-HBA at 25 μM reduced the expression of catabolic (MMP-1, MMP-3, MMP-13) and pro-inflammatory (COX-2) genes, while inducing the expression of anabolic markers (COL-II, ACAN), thereby exhibiting anti-catabolic, anti-inflammatory, and pro-anabolic activities.[56] In addition, 4-HBA at 50 mg kg^{-1} has been shown to attenuate the levels of key inflammatory cytokines, including IL-1β, TNF-α, and IL-6, in mice exposed to LPS-induced septic shock.[57] Altogether, these compounds constitute a phytochemical blend endowed with anti-inflammatory and chondroprotective properties, underscoring *Curcuma caesia* Roxb. as a promising nutraceutical candidate for OA management. In particular, given the reported NLRP3-inhibitory, Nrf2-activating, and $\Delta\Psi_m$-preserving effects of specific phenolic acids, including VA and 4-HBA, the retained chondroprotective activity of dBTE may be partly attributed to the persistence of these compounds within the bioaccessible fraction[53,56,58]

Another possible explanation supporting the biological activity of dBTE involves synergistic interactions among the identified phenolics after simulated digestion. Indeed, although only partially bioaccessible, flavan-3-ols such as EC and PB2 remained detectable after digestion and may still contribute to the overall chondroprotective activity of dBTE, together with other classes of phenolic compounds, including flavonols, phenolic acids, and anthocyanins, thereby generating biological effects beyond the individual mechanisms of each constituent.[59] Alternatively, other non-phenolic bioactive compounds potentially retained after simulated digestion, including phytosterols and terpenes, may also contribute to the observed chondroprotective activity of dBTE.[60,61] In addition, although not considered in the present study, intestinal microbiota may transform BTE polyphenols into bioactive phenolic metabolites that could contribute to the overall biological effects observed following digestion.[62] Moreover, polyphenols can interact with polysaccharides and proteins within the food matrix, forming complexes that may affect their extractability, stability, and bioaccessibility. During *in vitro* digestion, factors such as pH variations and digestive enzymes may facilitate the disruption of such interactions, potentially impacting the release and bioaccessibility of phenolic compounds.[63] In this regard, such matrix-related interactions may partly contribute to the release of phenolics within dBTE, potentially affecting its observed chondroprotective activity despite its lower overall phenolic content. Polyphenols are typically characterized by limited bioaccessibility, which may constrain the translational potential of phenolic-rich ingredients for health-related applications. Investigating polyphenol bioaccessibility is thus essential to quantify the phenolic fraction

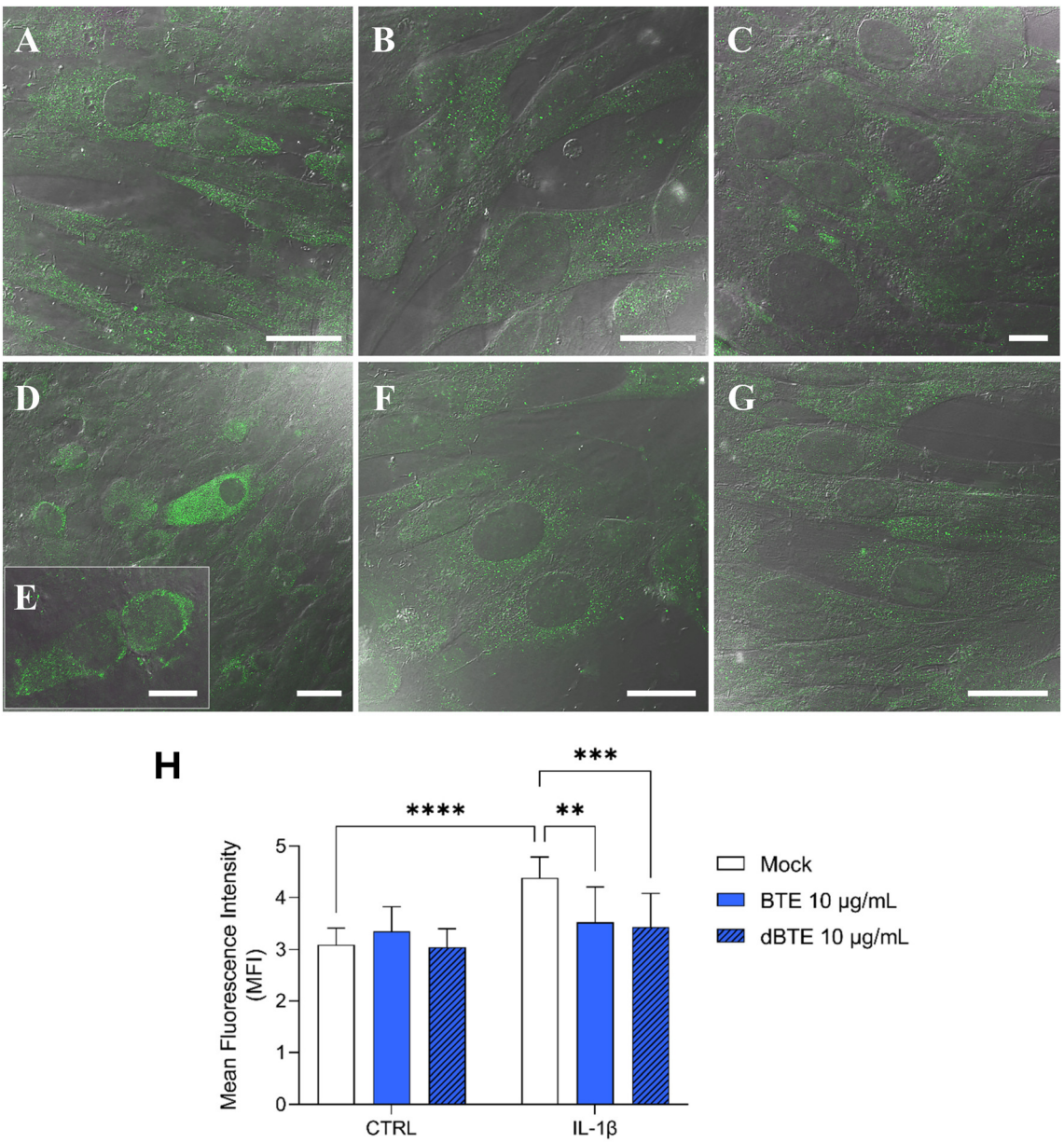

Fig. 10 Assessment of NLRP3 activation in C-28/I2 cells under different conditions. CLSM analysis of NLRP3 fluorescence in C-28/I2 cells under various conditions: untreated controls (A), BTE- and dBTE-treated cells (B and C), IL-1β-exposed cells (D and E), and IL-1β-exposed cells pre-treated with BTE or dBTE (F and G). Scale bar: 25 μm for A, B, C, D, F and G, 10 μm for E. Quantification of NLRP3 fluorescence intensity is shown in panel H. Data are expressed as Mean Fluorescence Intensity (MFI), and the results are presented as mean ± SD from eleven distinct, non-overlapping fields for each condition. Statistical analysis was performed using ordinary two-way ANOVA, Šídák's multiple comparison test, $^{*}P$ value <0.05, $^{**}P < 0.01$, $^{***}P < 0.001$, $^{****}P < 0.0001$.

soluble in the digestive fluids and, therefore, potentially available for intestinal absorption. In this context, *in vitro* gastrointestinal digestion is widely employed to estimate the bioaccessibility of bioactive compounds within complex food matrices. HPLC-MS/MS analysis revealed a total polyphenol content of 3523.04 mg kg^{-1}. Notably, following simulated gastrointestinal digestion, this amount decreased to 2053.43 mg kg^{-1}, indicating an overall polyphenol bioaccessibility of 58.3%. Nevertheless, phenolic retention during digestion was strictly compound-dependent, encompassing both highly stable and degradation-prone polyphenols. Flavan-3-ols were the most digestion-sensitive compounds: catechin, epicatechin, and procyanidin B2 showed retentions of 13.1%, 38.7%, and 47.2%, respectively. Overall, the flavan-3-ol fraction decreased from 1437.50 to 534.67 mg kg^{-1}, corresponding to approximately 37.2% retention. Conversely, hydroxybenzoic acids were comparatively more stable. 4-Hydroxybenzoic and syringic acids showed almost complete retention, 95.5% and 95.6%, respectively. As a class, hydro-

xybenzoic acids decreased from 1444.23 to 1168.02 mg kg^{-1}, corresponding to about 80.9% retention, and represented approximately 56.9% of the phenolic profile of dBTE. Hydroxycinnamic acids showed an intermediate behaviour with about 54.0% retention, although *p*-coumaric and ferulic acids were markedly reduced. In line with these findings, Ozkan *et al.* reported reduced epicatechin levels in *Crataegus monogyna* Jacq. and *Crataegus orientalis* Pall herbs during *in vitro* gastrointestinal digestion. Such reduced contents may be attributed to degradation processes driven by pH variations within the digestive fluids, bile acid-mediated precipitation, as well as polyphenol autoxidation, polymerization, and epimerization.[57] This compound-dependent profile has direct implications for the development of blue turmeric-based functional foods. Formulation should be guided by the bioaccessible phenolic fingerprint after digestion. In this perspective, hydroxybenzoic acids may represent digestion-resilient markers for standardization, whereas flavan-3-ols should be considered bioactive but digestion-labile compounds that may require formulation strategies aimed at improving stability and release. Notably, among the identified BTE phenolic compounds, isoquercitrin, procyanidin A2, and delphinidin 3-galactoside showed increased levels after digestion. As previously reported, enhanced apparent bioaccessibility may arise from the release of phenolic compounds from food matrix components, such as dietary fibers and proteins, during digestion, thereby increasing their solubility in intestinal fluids.[64,65] Recent studies have demonstrated that matrix composition markedly affects the bioaccessibility of phenolic compounds, including anthocyanins, whose behavior may be influenced by lipids, proteins, and polysaccharides.[66,67] In our study, the impact of digestion on anthocyanin levels was compound-dependent, with delphinidin 3,5-diglucoside decreasing following digestion, whereas delphinidin 3-galactoside, undetected in the parent methanolic extract, became detectable in the bioaccessible fraction. Such variations may arise from the distinct chemical environments associated with BTE and dBTE preparation, which could alter anthocyanin detectability through inter- and intra-molecular interactions occurring within complex chemical microenvironments. In this regard, transformations of acylated anthocyanins during gastrointestinal digestion have been reported to modify anthocyanin profiles and influence their detectability.[68–70] Moreover, digestion-related chemical transformations of parent phenolics may be involved in variations in the detectable anthocyanin profile. Consistently, Kim *et al.* reported that specific anthocyanins and anthocyanidins became detectable or increased after *in vitro* digestion due to transformations of parent compounds.[71] In addition, the process of *in vitro* digestion may behave as a biological extraction system, comprising enzymes, bile salts, electrolytes, and pH variations, which may impact the release and extractability of phenolics. For instance, variations in the protonation/deprotonation state of phenolics have been reported to influence their oxidative status and stability, thereby affecting their extractability.[72] Lastly, some apparent increases in specific phenolic compounds may also reflect matrix-related analytical effects, including ion suppression or ion enhancement, which can affect the quantification of target analytes or potentially contribute to analytical artifacts.[73] Overall, these findings indicate that gastrointestinal digestion deeply impacts the bioaccessibility of the phenolic fraction of *Curcuma caesia* Roxb, without significantly reducing the overall effectiveness of the phytocomplex in mitigating OA-related inflammation. Nevertheless, several phenolics were substantially reduced after digestion and specific biological effects, such as mitochondrial mass preservation, were partially compromised. This suggests that further optimization may enhance the overall bioaccessibility and bioactivity of BTE phenolics. In this regard, microbial fermentation of functional foods represents a valuable approach to improve bioaccessibility and functional properties of natural bioactive compounds. During fermentation, secreted microbial enzymes such as cellulase, tannase, pectinase, and β-glucosidase can drive alterations in the composition and bioactivity of food-derived phenolic compounds. Fan *et al.* reported extensive biotransformation of epigallocatechin gallate (EGCG) following exposure to the fungus *Eurotium cristatum*, resulting in increased total phenolic content (TPC), total flavonoid content (TFC), and antioxidant capacity through the bioconversion of EGCG into metabolites such as epigallocatechin (EGC) and gallic acid (GA), and other theaflavin-type compounds.[74] Likewise, Massaro *et al.* demonstrated that lactic acid bacteria (LAB)-driven fermentation of *Malva sylvestris* extract resulted in a threefold increase in TPC and a twofold increase in antioxidant activity compared with the unfermented extract, together with a pronounced reduction in tannin levels and an overall improvement in antimicrobial bioactivity.[75] In this context, microbial fermentation of *Curcuma caesia* extracts may increase the total content of phenolics and enhance their functional effects by increasing the availability of these compounds in digestive fluids. For instance, the bioconversion of phenolic acids by microbial reductases and decarboxylases may result in the accumulation of corresponding dihydro-derivatives with enhanced availability in digestive fluids, potentially facilitating their absorption, bioavailability, and bioactivity, thereby increasing the intrinsic functional value of *Curcuma caesia* phenolics.[76] Although no human pharmacokinetic data are available for blue turmeric and no standardized daily intake has been established for this novel spice, a bioaccessibility-adjusted calculation based on HPLC-MS/MS data and the active concentration range (5–50 μg mL^{-1}) can provide a preliminary indication of the translational relevance of the extract doses. BTE and dBTE contain 3523.04 mg kg^{-1} and 2053.43 mg kg^{-1} of phenolic compounds, respectively. Accordingly, the tested concentration range (5–50 μg mL^{-1}) corresponds to about 16.6–176.2 ng mL^{-1} of phenolics for BTE and 10.3–102.7 ng mL^{-1} for dBTE, whereas at 10 μg mL^{-1} the corresponding concentrations are approximately 35.2 ng mL^{-1} and 20.5 ng mL^{-1}, respectively. These values should not be interpreted as direct plasma-equivalent concentrations of unchanged extract, but rather as the concentrations of quantified phenolic compounds to which cells were exposed within the complex extract mixture. This is relevant because human studies on dietary polyphenols generally report low systemic exposure to parent compounds, with circulating concentrations often in the nM to μM range and with extensive contri-

bution of phase-II conjugates and microbiota-derived metabolites. Therefore, the present data support a mechanistic and preclinical rationale, but they do not yet define an effective human intake. If BTE were developed as a nutraceutical ingredient, the estimated amount of bioaccessible phenolics may be approximated based on the measured phenolic content of dBTE and the intended daily oral dose: bioaccessible phenolics (mg day^{-1}) = oral BTE dose (mg day^{-1}) × 2.053 μg mg^{-1} ÷ 1000. However, if dried rhizome powder is used, this calculation should include the extraction yield from the raw material.

Finally, while the evaluation of phenolic bioaccessibility through *in vitro* simulated digestion provides valuable information regarding the digestive fate of BTE phenolics, further investigations, including post-digestive microbial biotransformation models and Caco-2-based intestinal epithelial absorption models, are warranted to characterize the actual bioavailability of BTE phenolic compounds.

5. Conclusions

Overall, the present study identifies blue turmeric phenolics as promising bioactives for the management of OA-related inflammation, retaining relevant bioactivity following simulated digestion. Notably, the overall polyphenol bioaccessibility after *in vitro* digestion was 58%. From a functional perspective, both parent and digested extracts exerted protective effects in IL-1β-stimulated human chondrocytes within a concentration range of 5–50 μg mL^{-1} through modulation of inflammatory and oxidative stress pathways, including TNF-α suppression and Nrf2 activation, while preserving mitochondrial function, cell viability, and regenerative potential. However, the translational relevance of these findings remains limited by several aspects: (i) the *in vitro* digestion model used in this study does not account for colonic microbial metabolism of phenolics; (ii) intestinal epithelial transport and absorption of BTE phenolics were not evaluated; (iii) the OA model based on immortalized chondrocytes only partially reflects the complexity of the human articular cartilage microenvironment; and (iv) BTE functional activities have not yet been evaluated *in vivo*. Therefore, further studies are warranted to better characterize BTE bioactivity in more complex OA models (synovial cultures, osteochondral explants, genetic mouse models), assess potential synergistic or additive interactions among phenolics and related metabolites, perform toxicological assessment in accordance with EFSA guidelines, and evaluate the incorporation of BTE into real food matrices.

Author contributions

Matteo Micucci (MM); Federico Gianfanti (FG); Michela Battistelli (MB); Giovanni Caprioli (GC): writing – review & editing, writing – original draft. MM: funding acquisition. MM; FG; MB conceptualization. Elena Barbieri (EB); Agnese Santanatoglia (AS); Michele Mari (MMA); Michele Retini (MR); Maria Assunta Meli (MAM); Carla Roselli (CR); Fabio Ferrini (FF); Riham Osman (RO); Sabrina Burattini (SB); Francesco Onesimo (FO): investigation. EB; AS; MMA; MR; MAM; CR; FF; RO; SB; MB; FG; MM: data curation. MM; FG; MB: supervision, project administration.

Conflicts of interest

There are no conflicts to declare.

Data availability

The data used to support the findings of this study are included within the article and are available from the corresponding author upon request.

Supplementary information (SI) is available. See DOI: https://doi.org/10.1039/d6fo02399a.

Acknowledgements

This work was supported by the Italian Ministry of University and Research (MUR) under the PRIN2022 program (Project PRIN2022_CTC, Grant No. 2022FHF5BE).

References

1 T. Sakai, F. Kambe, H. Mitsuyama, N. Ishiguro, K. Kurokouchi, M. Takigawa, H. Iwata and H. Seo, Tumor Necrosis Factor α Induces Expression of Genes for Matrix Degradation in Human Chondrocyte-like HCS-2/8 Cells Through Activation of NF-κB: Abrogation of the Tumor Necrosis Factor α Effect by Proteasome Inhibitors, *J. Bone Miner. Res.*, 2001, **16**, 1272–1280.

2 A. Liacini, Induction of matrix metalloproteinase-13 gene expression by TNF-α is mediated by MAP kinases, AP-1, and NF-κB transcription factors in articular chondrocytes, *Exp. Cell Res.*, 2003, **288**, 208–217.

3 J. Park, H. Park, Y. Lee, S. Weon, Y.-G. Kim, J.-H. Yang, B. Nam, S. Jo and T.-H. Kim, Blocking TNFα attenuates progressive cartilage matrix degradation in inflammatory arthritis, *Exp. Ther. Med.*, 2021, **22**, 808.

4 E. Altobelli, P. M. Angeletti, D. Piccolo and R. De Angelis, Synovial Fluid and Serum Concentrations of Inflammatory Markers in Rheumatoid Arthritis, Psoriatic Arthritis and Osteoarthitis: A Systematic Review, *Curr. Rheumatol. Rev.*, 2017, **13**, 170–179.

5 A. J. Schuerwegh, E. J. Dombrecht, W. J. Stevens, J. F. Van Offel, C. H. Bridts and L. S. De Clerck, Influence of pro-inflammatory (IL-1α, IL-6, TNF-α, IFN-γ) and anti-inflammatory (IL-4) cytokines on chondrocyte function, *Osteoarthr. Cartil.*, 2003, **11**, 681–687.

6 C. Cheung, S. Tu, Y. Feng, C. Wan, H. Ai and Z. Chen, Mitochondrial quality control dysfunction in osteoarthritis:

Mechanisms, therapeutic strategies & future prospects, *Arch. Gerontol. Geriatr.*, 2024, **125**, 105522.
7 P. Lepetsos, K. A. Papavassiliou and A. G. Papavassiliou, Redox and NF-κB signaling in osteoarthritis, *Free Radicals Biol. Med.*, 2019, **132**, 90–100.
8 A. Sharma, S. Jagga, S.-S. Lee and J.-S. Nam, Interplay between Cartilage and Subchondral Bone Contributing to Pathogenesis of Osteoarthritis, *Int. J. Mol. Sci.*, 2013, **14**, 19805–19830.
9 R. Patusco, K. Gyasi and A. Kaufmann, Exploring the nexus between inflammation and mobility through the lens of healthy aging: current scenario and future perspectives, *Aging:Clin. Exp. Res.*, 2026, **38**, 60.
10 Y. Abu-Amer, Cross-regulation of inflammation and metabolic mechanisms in osteoarthritis: recent advances bridging the gap to novel treatments, *Connect. Tissue Res.*, 2025, **66**, 339–344.
11 C. Palazzo, C. Nguyen, M.-M. Lefevre-Colau, F. Rannou and S. Poiraudeau, Risk factors and burden of osteoarthritis, *Ann. Phys. Rehabil. Med.*, 2016, **59**, 134–138.
12 I. Morales-Ivorra, M. Romera-Baures, B. Roman-Viñas and L. Serra-Majem, Osteoarthritis and the Mediterranean Diet: A Systematic Review, *Nutrients*, 2018, **10**, 1030.
13 N. Veronese, B. Stubbs, M. Noale, M. Solmi, C. Luchini, T. O. Smith, C. Cooper, G. Guglielmi, J.-Y. Reginster, R. Rizzoli and S. Maggi, Adherence to a Mediterranean diet is associated with lower prevalence of osteoarthritis: Data from the osteoarthritis initiative, *Clin. Nutr.*, 2017, **36**, 1609–1614.
14 D. Zhao, S. Shen, Y. Guo, Y. Wang, C. Gu, B. Guo and T. Jiang, Flavan-3-ol monomers intake is associated with osteoarthritis risk in Americans over 40 years of age: results from the National Health and Nutritional Examination Survey database, *Food Funct.*, 2024, **15**, 6966–6974.
15 E.-S. Scarpa, A. Antonelli, G. Balercia, S. Sabatelli, F. Maggi, G. Caprioli, G. Giacchetti and M. Micucci, Antioxidant, Anti-Inflammatory, Anti-Diabetic, and Pro-Osteogenic Activities of Polyphenols for the Treatment of Two Different Chronic Diseases: Type 2 Diabetes Mellitus and Osteoporosis, *Biomolecules*, 2024, **14**, 836.
16 M. H. Farzaei, A. K. Singh, R. Kumar, C. R. Croley, A. K. Pandey, E. Coy-Barrera, J. Kumar Patra, G. Das, R. G. Kerry, G. Annunziata, G. C. Tenore, H. Khan, M. Micucci, R. Budriesi, S. Momtaz, S. M. Nabavi and A. Bishayee, Targeting Inflammation by Flavonoids: Novel Therapeutic Strategy for Metabolic Disorders, *Int. J. Mol. Sci.*, 2019, **20**, 4957.
17 M. Y. Ansari, N. Ahmad and T. M. Haqqi, Oxidative stress and inflammation in osteoarthritis pathogenesis: Role of polyphenols, *Biomed. Pharmacother.*, 2020, **129**, 110452.
18 M. Sirše, Effect of Dietary Polyphenols on Osteoarthritis—Molecular Mechanisms, *Life*, 2022, **12**, 436.
19 E. Valsamidou, A. Gioxari, C. Amerikanou, P. Zoumpoulakis, G. Skarpas and A. C. Kaliora, Dietary Interventions with Polyphenols in Osteoarthritis: A Systematic Review Directed from the Preclinical Data to Randomized Clinical Studies, *Nutrients*, 2021, **13**, 1420.
20 A. Maouche, K. Boumediene and C. Baugé, Bioactive Compounds in Osteoarthritis: Molecular Mechanisms and Therapeutic Roles, *Int. J. Mol. Sci.*, 2024, **25**, 11656.
21 M. Sirše, Effect of Dietary Polyphenols on Osteoarthritis-Molecular Mechanisms, *Life*, 2022, **12**, 436.
22 D. R. Omotoso and O. Aderinto, Harnessing the therapeutic potential of selected natural products in combating osteoarthritis using experimental model – A review, *Pharmacol. Res.*, 2025, **7**, 100276.
23 M. Micucci, B.-Z. Xiang, C.-M. Ting, H.-Y. Kwan, M. Mari, M. Retini, S. Burattini, R. Osman, U. J. Okeke, F. O. Abdullah, F. Gianfanti and M. Battistelli, Matching traditional Chinese medicine and western medicine-based research: Advanced nutraceutical development for proactive gastric cancer prevention, *World J. Gastrointest. Oncol.*, 2024, **16**, 3798–3819.
24 P.-W. Hou, P.-K. Fu, H.-C. Hsu and C.-L. Hsieh, Traditional Chinese medicine in patients with osteoarthritis of the knee, *J. Tradit. Complementary Med.*, 2015, **5**, 182–196.
25 R. Mallamaci, R. Budriesi, M. L. Clodoveo, G. Biotti, M. Micucci, A. Ragusa, F. Curci, M. Muraglia, F. Corbo and C. Franchini, Olive Tree in Circular Economy as a Source of Secondary Metabolites Active for Human and Animal Health Beyond Oxidative Stress and Inflammation, *Molecules*, 2021, **26**, 1072.
26 R. Aldini, R. Budriesi, G. Roda, M. Micucci, P. Ioan, A. D'Errico-Grigioni, A. Sartini, E. Guidetti, M. Marocchi, M. Cevenini, F. Rosini, M. Montagnani, A. Chiarini and G. Mazzella, Curcuma longa Extract Exerts a Myorelaxant Effect on the Ileum and Colon in a Mouse Experimental Colitis Model, Independent of the Anti-Inflammatory Effect, *PLoS One*, 2012, **7**, e44650.
27 A. Chiarini, M. Micucci, M. Malaguti, R. Budriesi, P. Ioan, M. Lenzi, C. Fimognari, T. Gallina Toschi, P. Comandini and S. Hrelia, Sweet Chestnut (*Castanea sativa* Mill.) Bark Extract: Cardiovascular Activity and Myocyte Protection against Oxidative Damage, *Oxid. Med. Cell. Longevity*, 2013, **2013**, 1–10.
28 E. Chiaino, R. Stella, C. Peggion, M. Micucci, R. Budriesi, L. B. Mattioli, C. Marzetti, F. Pessina, M. Valoti and M. Frosini, Acacia catechu Willd. Extract Protects Neuronal Cells from Oxidative Stress-Induced Damage, *Antioxidants*, 2021, **11**, 81.
29 C. Roselli, D. Desideri, L. Feduzi, L. Ugolini and M. A. Meli, Application of an *in vitro* digestion model for ^{210}Po bioaccessibility assessment in seafood, *J. Radiol. Prot.*, 2017, **37**, 907–917.
30 M. Micucci, M. Battistelli, S. Burattini, R. Osman, F. Onesimo, M. Mari, M. Retini, I. Versari, B. Pagliarani, A. Tarozzi, G. Zappia, F. Gianfanti and L. Pruccoli, Antioxidant and neuroprotective effects of ubiquinol diacetate: Insights from SH-SY5Y cell line and Caenorhabditis elegans models of Parkinson's disease, *Exp. Mol. Pathol.*, 2026, **145**, 105023.
31 M. Micucci, G. Caprioli, I. Versari, L. Acquaticci, G. Sagratini, F. Gianfanti, F. Onesimo, I. Faenza,

S. Burattini, M. Mari, M. Retini, R. Osman, S. Salucci and M. Battistelli, Blackthorn juice from central Italy exhibits selective anticancer activity by inducing apoptosis and autophagy in gastric carcinoma cells, *Food Funct.*, 2025, **16**, 8548–8563.

32 M. Micucci, M. Battistelli, S. Burattini, M. Mari, M. Retini, R. Osman, I. Versari, A. B. Stella, F. Gianfanti, J. O. Udodinma, F. Onesimo, S. Riela, M. Canale, A. P. Piccionello, I. Faenza and S. Salucci, Food Waste to Wellness: A Grape Pomace Blend in Gastric Cancer Prevention, *Food Sci. Nutr.*, 2025, **13**, e70350.

33 J. A. Garcia-Merino, V. Carrabs, F. Ferrini, S. Salucci, M. Battistelli, S. Burattini, F. Luchetti, M. G. Nasoni, G. Annibalini, M. Micucci, F. Gianfanti, P. Sestili, M. Larrosa and E. Barbieri, Revitalizing Muscle Regeneration: Cocoa Polyphenols Shield Mitochondrial Integrity and Boost Myogenesis Under Oxidative Stress, *Microsc. Res. Tech.*, 2025, **88**, 905–912.

34 E. Grassi, A. Cocozza di Montanara, M. Battistelli, M. Micucci, L. Guidi, F. Gianfanti, E. Baldrighi, L. Catani, R. Sandulli and F. Semprucci, Caenorhabditis elegans in the research of plants-derived nutraceuticals: a VOSviewer-based trend analysis, *Heliyon*, 2025, **11**, e43595.

35 A. Gironés-Vilaplana, P. Valentão, D. A. Moreno, F. Ferreres, C. García-Viguera and P. B. Andrade, New Beverages of Lemon Juice Enriched with the Exotic Berries Maqui, Açaí, and Blackthorn: Bioactive Components and in Vitro Biological Properties, *J. Agric. Food Chem.*, 2012, **60**, 6571–6580.

36 M. J. Dehzad, H. Ghalandari, M. Nouri and M. Askarpour, Antioxidant and anti-inflammatory effects of curcumin/turmeric supplementation in adults: A GRADE-assessed systematic review and dose–response meta-analysis of randomized controlled trials, *Cytokine*, 2023, **164**, 156144.

37 S. K. Vanga, A. Singh and V. Raghavan, Review of conventional and novel food processing methods on food allergens, *Crit. Rev. Food Sci. Nutr.*, 2017, **57**, 2077–2094.

38 Y. Liu, S. S. Roy, R. H. C. Nebie, Y. Zhang and M. G. Nair, Functional Food Quality of Curcuma caesia, Curcuma zedoaria and Curcuma aeruginosa Endemic to Northeastern India, *Plant Foods Hum. Nutr.*, 2013, **68**, 72–77.

39 N. N. A. Ibrahim, W. A. Wan Mustapha, N.-S. Sofian-Seng, S. J. Lim, N. S. Mohd Razali, A. H. Teh, H. A. Rahman and A. Mediani, A Comprehensive Review with Future Prospects on the Medicinal Properties and Biological Activities of *Curcuma caesia* Roxb., *Evidence-Based Complementary Altern. Med.*, 2023, **2023**, 7006565.

40 S. Burattini, F. Gianfanti, F. Onesimo, S. D. Zeppa, B. Canonico, M. Montanari, G. Panza, D. Lopez, G. Annibalini, F. Fanelli, R. Saltarelli, M. Mari, M. Retini, R. Osman, A. Mariam, M. Micucci, G. Caprioli, A. Santanatoglia, D. Agostini and M. Battistelli, Blue elixir of youth and wellness: The multicomponent-multitarget paradigm of *Curcuma caesia* Roxb, *J. Funct. Foods*, 2025, **125**, 106699.

41 A. G. Oomen, C. J. M. Rompelberg, M. A. Bruil, C. J. G. Dobbe, D. P. K. H. Pereboom and A. J. A. M. Sips, Development of an In Vitro Digestion Model for Estimating the Bioaccessibility of Soil Contaminants, *Arch. Environ. Contam. Toxicol.*, 2003, **44**, 281–287.

42 A. Santanatoglia, G. Caprioli, M. Cespi, D. Ciarlantini, L. Cognigni, L. Fioretti, F. Maggi, A. M. Mustafa, F. Nzekoue and S. Vittori, A comprehensive comparative study among the newly developed Pure Brew method and classical ones for filter coffee production, *LWT – Food Sci. Technol.*, 2023, **175**, 114471.

43 F. Finger, C. Schörle, A. Zien, P. Gebhard, M. B. Goldring and T. Aigner, Molecular phenotyping of human chondrocyte cell lines T/C–28a2, T/C–28a4, and C–28/I2, *Arthritis Rheum.*, 2003, **48**, 3395–3403.

44 M. B. Goldring, J. R. Birkhead, L. F. Suen, R. Yamin, S. Mizuno, J. Glowacki, J. L. Arbiser and J. F. Apperley, Interleukin-1 beta-modulated gene expression in immortalized human chondrocytes., *J. Clin. Invest.*, 1994, **94**, 2307–2316.

45 F. Ferrini, S. Donati Zeppa, D. Fraternale, V. Carrabs, G. Annibalini, G. Verardo, A. Gorassini, M. C. Albertini, T. Ismail, C. Fimognari and P. Sestili, Characterization of the Biological Activity of the Ethanolic Extract from the Roots of Cannabis sativa L, Grown in Aeroponics, *Antioxidants*, 2022, **11**, 860.

46 Y. Li, Y. Yang, J. Guo, X. Guo, Z. Feng and X. Zhao, Spinal NF-kB upregulation contributes to hyperalgesia in a rat model of advanced osteoarthritis, *Mol. Pain*, 2020, **16**, 1–12.

47 K. S. Alharbi, O. Afzal, A. S. A. Altamimi, W. H. Almalki, I. Kazmi, F. A. Al-Abbasi, S. I. Alzarea, H. A. Makeen and M. Albratty, Potential role of nutraceuticals via targeting a Wnt/β–catenin and NF–κB pathway in treatment of osteoarthritis, *J. Food Biochem.*, 2022, **46**, e14427.

48 Y. He, H. Hara and G. Núñez, Mechanism and Regulation of NLRP3 Inflammasome Activation, *Trends Biochem. Sci.*, 2016, **41**, 1012–1021.

49 F. Shahidi and A. Samarasinghe, How to assess antioxidant activity? Advances, limitations, and applications of in vitro, in vivo, and ex vivo approaches, *Food Prod., Process. Nutr.*, 2025, **7**, 50.

50 K. Lee, S. Bharadwaj, U. Yadava and S. Kang, Computational and In Vitro Investigation of (-)-Epicatechin and Proanthocyanidin B2 as Inhibitors of Human Matrix Metalloproteinase 1, *Biomolecules*, 2020, **10**, 1379.

51 I. Cordero-Herrera, X. Chen, S. Ramos and S. Devaraj, (−)-Epicatechin attenuates high-glucose-induced inflammation by epigenetic modulation in human monocytes, *Eur. J. Nutr.*, 2017, **56**, 1369–1373.

52 W. Cai, Y. Zhang, W. Jin, S. Wei, J. Chen, C. Zhong, Y. Zhong, C. Tu and H. Peng, Procyanidin B2 ameliorates the progression of osteoarthritis: An in vitro and in vivo study, *Int. Immunopharmacol.*, 2022, **113**, 109336.

53 Z. Ma, Z. Huang, L. Zhang, X. Li, B. Xu, Y. Xiao, X. Shi, H. Zhang, T. Liao and P. Wang, Vanillic Acid Reduces Pain-Related Behavior in Knee Osteoarthritis Rats Through the

Inhibition of NLRP3 Inflammasome-Related Synovitis, *Front. Pharmacol.*, 2021, **11**, 599022.
54 X. Huang, Y. Xi, Z. Mao, X. Chu, R. Zhang, X. Ma, B. Ni, H. Cheng and H. You, Vanillic acid attenuates cartilage degeneration by regulating the MAPK and PI3K/AKT/NF-κB pathways, *Eur. J. Pharmacol.*, 2019, **859**, 172481.
55 R. Ziadlou, A. Barbero, M. J. Stoddart, M. Wirth, Z. Li, I. Martin, X. Wang, L. Qin, M. Alini and S. Grad, Regulation of Inflammatory Response in Human Osteoarthritic Chondrocytes by Novel Herbal Small Molecules, *Int. J. Mol. Sci.*, 2019, **20**, 5745.
56 Y. Kou, Q. Jing, X. Yan, J. Chen, Y. Shen, Y. Ma, Y. Xiang, X. Li, X. Liu, Z. Liu, Y. Wei and Y. Wang, 4-Hydroxybenzoic acid restrains Nlrp3 inflammasome priming and activation via disrupting PU.1 DNA binding activity and direct antioxidation, *Chem.-Biol. Interact.*, 2024, **404**, 111262.
57 G. Ozkan, F. B. Sakarya, D. Tas, B. Yurt, S. Ercisli and E. Capanoglu, Effect of *In Vitro* Digestion on the Phenolic Content of Herbs Collected from Eastern Anatolia, *ACS Omega*, 2023, **8**, 12730–12738.
58 Y. Gong, J. Ye, T. Jiang, S. Shao, S. Li, Z. Li, J. Qiu, X. Zheng, B. Zheng, C. Jiang, H. Chen and Z. Hong, KLF2-Mediated Modulation of oxidative stress and pyroptosis by Vanillic acid in intervertebral disc degeneration, *Biochem. Pharmacol.*, 2026, **249**, 117907.
59 L. K. Caesar and N. B. Cech, Synergy and antagonism in natural product extracts: when 1 + 1 does not equal 2, *Nat. Prod. Rep.*, 2019, **36**, 869–888.
60 S. J. P. Sampath, S. N. Rath, N. Kotikalapudi and V. Venkatesan, Beneficial effects of secretome derived from mesenchymal stem cells with stigmasterol to negate IL-1β-induced inflammation *in vitro* using rat chondrocytes-OA management, *Inflammopharmacology*, 2021, **29**, 1701–1717.
61 A. M. S. Carvalho, L. Heimfarth, K. A. Santos, A. G. Guimarães, L. Picot, J. R. G. S. Almeida, J. S. S. Quintans and L. J. Quintans-Júnior, Terpenes as possible drugs for the mitigation of arthritic symptoms - A systematic review, *Phytomedicine*, 2019, **57**, 137–147.
62 S. Langa, J. A. Curiel, R. de la Bastida, Á. Peirotén and J. M. Landete, Importance of interaction between the matrix effect and microbial metabolism in the bioavailability of lignans, *J. Sci. Food Agric.*, 2026, **106**, 2180–2189.
63 F. Shahidi and K. D. Athiyappan, Polyphenol-polysaccharide interactions: molecular mechanisms and potential applications in food systems - a comprehensive review, *Food Prod., Process. Nutr.*, 2025, **7**, 42.
64 Y. Qin, L. Wang, Y. Liu, Q. Zhang, Y. Li and Z. Wu, Release of phenolics compounds from Rubus idaeus L. dried fruits and seeds during simulated in vitro digestion and their bio-activities, *J. Funct. Foods*, 2018, **46**, 57–65.
65 K. Kasprzak-Drozd, J. Mołdoch, M. Gancarz, A. Wójtowicz, I. Kowalska, T. Oniszczuk and A. Oniszczuk, In Vitro Digestion of Polyphenolic Compounds and the Antioxidant Activity of Acorn Flour and Pasta Enriched with Acorn Flour, *Int. J. Mol. Sci.*, 2024, **25**, 5404.
66 D. M. Ribnicky, D. E. Roopchand, A. Oren, M. Grace, A. Poulev, M. A. Lila, R. Havenaar and I. Raskin, Effects of a high fat meal matrix and protein complexation on the bioaccessibility of blueberry anthocyanins using the TNO gastrointestinal model (TIM-1), *Food Chem.*, 2014, **142**, 349–357.
67 H. Xue, M. Zha, Y. Tang, J. Zhao, X. Du and Y. Wang, Research Progress on the Extraction and Purification of Anthocyanins and Their Interactions with Proteins, *Molecules*, 2024, **29**, 2815.
68 J. Wang, Y. Zhao, B. Sun, Y. Yang, S. Wang, Z. Feng and J. Li, The structure of anthocyanins and the copigmentation by common micromolecular copigments: A review, *Food Res. Int.*, 2024, **176**, 113837.
69 P. de Aguiar Cipriano, H. Kim, C. Fang, V. P. Venancio, S. U. Mertens-Talcott and S. T. Talcott, In vitro digestion, absorption and biological activities of acylated anthocyanins from purple sweet potatoes (Ipomoea batatas), *Food Chem.*, 2022, **374**, 131076.
70 J. Jokioja, B. Yang and K. M. Linderborg, Acylated anthocyanins: A review on their bioavailability and effects on postprandial carbohydrate metabolism and inflammation, *Compr. Rev. Food Sci. Food Saf.*, 2021, **20**, 5570–5615.
71 I. Kim, J. K. Moon, S. J. Hur and J. Lee, Structural changes in mulberry (Morus Microphylla. Buckl) and chokeberry (Aronia melanocarpa) anthocyanins during simulated in vitro human digestion, *Food Chem.*, 2020, **318**, 126449.
72 M. Mencin, N. Markanovič, M. Mikulič-Petkovšek, R. Veberič and P. Terpinc, Changes in the Bioaccessibility of Antioxidants after Simulated In Vitro Digestion of Bioprocessed Spelt-Enhanced Wheat Bread, *Antioxidants*, 2023, **12**, 487.
73 A. Nasiri, R. Jahani, S. Mokhtari, H. Yazdanpanah, B. Daraei, M. Faizi and F. Kobarfard, Overview, consequences, and strategies for overcoming matrix effects in LC-MS analysis: a critical review, *Analyst*, 2021, **146**, 6049–6063.
74 Z. Fan, Q. Qing, J. Yin, C. He, Y. Hu, Y. Chen, Y. Ren, M. Zhu, Z. Liu, X. Peng and Y. Xiao, Metabolites of epigallocatechin gallate and changes in antioxidant activity through biotransformation with Eurotium cristatum during liquid-state fermentation, *Food Chem.:X*, 2025, **29**, 102618.
75 S. Massaro, J. Sica, G. Ghion, C. Nadai, S. Vincenzi, D. Porcellato, V. Corich, A. Giacomini and A. Tarrah, Enhancing Malva sylvestris extract properties through lactic acid bacteria fermentation: impact on phytochemical profile and bioactivity, *Food Prod., Process. Nutr.*, 2025, **7**, 40.
76 P. Filannino, Y. Bai, R. D. Cagno and M. Gobbetti, M.G. Gänzle, Metabolism of phenolic compounds by Lactobacillus spp. during fermentation of cherry juice and broccoli puree, *Food Microbiol.*, 2015, **46**, 272–279.

